論文 / 著書情報
Article / Book Information

題目(和文)	EPR分光法によるイオン液体中の分子の回転拡散に関するアニオンサイズ依存性の解明
Title(English)	Anion size dependent hydrodynamic rotational diffusion of molecules in room temperature ionic liquids as studied by EPR spectroscopy
著者(和文)	三宅祐輔
Author(English)	Yusuke Miyake
出典(和文)	学位:博士(理学), 学位授与機関:東京工業大学, 報告番号:甲第8254号, 授与年月日:2011年3月26日, 学位の種別:課程博士, 審査員:渋谷 一彦,河合 明雄
Citation(English)	Degree:Doctor (Science), Conferring organization: Tokyo Institute of Technology, Report number:甲第8254号, Conferred date:2011/3/26, Degree Type:Course doctor, Examiner:,
学位種別(和文)	博士論文
Type(English)	Doctoral Thesis

Anion size dependent hydrodynamic rotational diffusion of molecules in room temperature ionic liquids as studied by EPR spectroscopy

Yusuke Miyake

Department of Chemistry

Graduate School of Science and Engineering

Tokyo Institute of Technology

2011

Contents

List of Figures, Tables, Charts and Scheme

Figures

Tables

Charts

Scheme

Chapter 1. Introduction

(1.1) Room temperature ionic liquids (RTILs)

Air and water stable room temperature ionic liquids (RTILs), which are composed entirely of cation and anion, have been studied extensively since 1990s.[1-4] One of the characteristic features of RTILs lies in great diversity that various properties such as viscosity can be widely controlled by a choice of cation and anion combinations. For example, viscosities of RTILs with imidazolium cation changes by a choice of anions which have different volumes shown in Figure 1.1. RTILs could be synthesized with various unique physicochemical properties including magnetic or photochromic nature.[5-11] RTILs are considered as powerful candidate media for electric battery and chemical solvent because of electrically conducting and nonvolatile properties. For these applications, it is quite important to acquire basic information on diffusion motion of solute in RTILs and solute-solvent interaction in RTILs. However, there remain many unknown problems on molecular diffusion in RTILs. For example, energy transfer reaction from excited triplet naphthalene to benzophenone is known as nearly diffusion-controlled reaction in organic solvents, but in a typical RTIL of $BmimPF_{6,}$[12] the reaction rate constant turns out to be about four times larger than the diffusion controlled rate constant.[13] Similar experimental results have been reported for other chemical reaction systems.[14,15]

To dissolve the reason why the chemical reactions observed in RTILs are different from those in conventional solvents, basic motion which are translational and rotational

dynamics for solutes in RTILs should be understood.

(1.2) Translational diffusion of solutes in RTILs

For translational diffusion of solutes in RTILs, several papers have been reported. Morgan *et al.* measured diffusivities of several smaller-sized gases in RTILs and determined the diffusion coefficients, D_T, by using a lag-time technique at 303 K.[16] According to Stokes-Einstein (SE) hydrodynamic theory, the relation with $D_T \propto T\eta^{-1}$. The D_T values were plotted against η for each gas solute in RTILs at 303 K and D_T values for each gas samples in imidazolium RTILs are found to be proportional to $\eta^{-0.6}$. This relation is different from that described by SE equation. Nishiyama *et al.* reported that D_T values of monoxide and some kinds of organic solutes such as benzophenone (BP) and benzophenone ketyl radical (BPK) in RTILs by transient grating spectroscopy.[17] Figure 1.2 shows D_T values plotted against $T\eta^{-1}$ for (a) BP and BPK, and (b) monoxide In the result, D_T values for larger-sized BP or BPK in RTILs and molecular solvents were proportional to $T\eta^{-1}$. On the other hand, D_T values for smaller-sized monoxide in RTIL and molecular solvents are proportional to $(T\eta^{-1})^{0.6}$ and do not obey SE equation. These results indicate translational diffusion is affected by solute size.

(1.3) Rotational diffusion of solutes in RTILs

(1.3.1) Hydrodynamic theory for rotational diffusion

Rotational diffusion for solutes in molecular solvents has been evaluated by hydrodynamic theory. First, the hydrodynamic theory for rotational diffusion is explained.[18,19] The simplest model of rotational diffusion is one where the tip of a vector defining the orientation of a molecule makes a random walk over the surface of a sphere: this is isotropic Brownian motion. The conditional probability $P(\theta, \varphi, t)$ that the reference vector is oriented along (θ, φ) at a time, t, after it initially lay along (0, 0) is given by the diffusion equation

$$\frac{dP(\theta,\phi,t)}{dt} = D_R\left\{\frac{1}{\sin\theta}\frac{\partial}{\partial\theta}\left(\sin\theta\frac{\partial}{\partial\theta}\right)+\frac{1}{\sin^2\theta}\frac{\partial^2}{\partial\phi^2}\right\}P(\theta,\phi,t) \qquad (1.1)$$

where D_R is the rotational diffusion coefficient, the fundamental quantity characterizing the motion. The angular operator in this equation is identical to that which occurs in the Schrödinger equation for the hydrogen atom and which determines the orbital angular momentum. Therefore, it comes that the solution of eq (1.1) is an expansion in the spherical harmonics, $Y_{l,m}(\theta, \varphi)$

$$P(\theta,\phi,t) = \sum_{l,m} c_{l,m} Y_{l,m}(\theta,\phi)\exp\{-l(l+1)D_R t\} \qquad (1.2)$$

It can be shown that the effect of the rotational diffusion is to make the average value of any angular function, F (θ, φ), which can be expressed in terms of spherical harmonics, decay according to

$$\langle F(t)\rangle = \langle F(0)\rangle\exp\{-l(l+1)D_R t\} \qquad (1.3)$$

The anisotropic quantities of interest here are second-rank tensors, thus $l = 2$ and the correlation time can be identified as

$$\tau_R = \frac{1}{6D_R} \qquad (1.4)$$

The diffusion coefficient relates to the rotational friction coefficient, f_R, through the Einstein formula

$$D_R = \frac{k_B T}{f_R} \qquad (1.5)$$

and if a macroscopic sphere rotates in viscous liquid, f_R is given by Stokes's law

$$f_R = 8\pi\eta r_0^3 \qquad (1.6)$$

where η is the shear viscosity of the solvent and r_0 the hydrodynamic radius of the diffusion particle, one obtains the Debye equation for the rotational correlation time, τ_R

$$\tau_R = \frac{4\pi r_0^3 \eta}{3k_B T} = \frac{V_p \eta}{k_B T} \qquad (1.7)$$

where V_p is the molecular volume determined by the hydrodynamic radius r_0.

(1.3.2) Rotational diffusion of solutes in traditional molecular solvents

It has been reported that rotational correlation times for many solutes in molecular solvents have been determined experimentally and fitted by those calculated based on eq (1.7) which is called as Stokes-Einstein-Debye (SED) equation. For example, it was reported that rotational diffusion for coumarin 153 was determined experimentally in

methanol and agreed with those calculated by SED equation.[20] The volume for coumarin 153 is 243 Å^3 and it is much larger than that for methanol of 36 Å^3. The relation between volumes of coumarin and methanol satisfies SED theory premises that the volume of solute is much larger than that of solvent molecule.

(1.3.3) Reports on rotational diffusion of solutes in RTILs

Many experimental papers on the rotational motion of solute in RTILs have been reported in the last decade.[21-39] Most of them are based on the fluorescence decay experiments to investigate the solvation and rotation dynamics of dye molecules in RTILs. For example, Jin *et al.*[31] measured the rotational correlation times of coumarin 153 in various RTILs by a time correlated single photon counting method. Figure 1.3 shows rotational correlation times, $<\tau_{rot}>$, of coumarin 153 in RTILs and molecular solvents at room temperature plotted vs (η/T). The $<\tau_{rot}>$ measured in RTILs are proportional to (η/T) and longer than the τ_R values calculated by hydrodynamic theory with slip boundary condition same as those for molecular solvents. If the rotational correlation times are longer than those calculated by the theory, it can be said that the rotational diffusion follows the theory. The details are explained in Chapter 4. Therefore, they concluded that the rotational correlation times follow hydrodynamic equation with slip boundary condition. These previous studies seem to suggest that the rotational diffusion dynamics of solute in RTILs is similar to that in conventional solvents. It should be of note here that the SED equation assumes continuum media for solvent.

Under this assumption, solvent molecule should be much smaller in size than solute. One of the important structural characteristics of RTILs is that one unit of solvent, which may be composed of anion, cation, and the ion pair, is usually larger than conventional organic solvent molecules. This feature suggests us that the simple SED equation holds only for larger-sized solute / smaller-sized solvent systems such as fluorescent dye molecules in RTILs. From this viewpoint, the rotation dynamics of smaller-sized solute is quite interesting. Unfortunately, it is rather difficult to study the rotation motion of small solute by observing the fluorescence in the condensed phase. Dahl *et al*. challenged to measure the rotational correlation time of small solute such as NCS^- in RTILs by observing the relaxation of the vibrational excited level.[40] However, the solute size was so small that the relaxation took place rapidly and the rotation motion was not observed. Yasaka *et al.* measured the rotational correlation times of D_2O and C_6D_6 in $BmimPF_6$ and BmimCl by NMR spectroscopy and concluded that the rotational activation energy is smaller than that calculated by the SED hydrodynamic equation.[24] In the present thesis, the rotational diffusion of small size solutes in RTILs was evaluated experimentally by using EPR spectroscopy.

(1.4) EPR spectroscopy

(1.4.1) Features of EPR spectroscopy

There are three reasons why EPR spectroscopy is chosen in the present research to study solute's dynamics in RTILs. The first reason lies in a time range of EPR transition.

In EPR, spin-spin relaxation time, T_2, is a few ns. Rotational diffusion rate of solute in the solution is expected to occur in the range between picoseconds and nanoseconds. Because they are close each other, the T_2 value is influenced by rotation which reflects the observed EPR spectrum. The rotational correlation times which range picoseconds for small size solutes can be evaluated by an EPR method. The scond reason lies in the high selectivity for paramagnetic species. EPR provides information only on paramagnetic species and their surroundings. If radicals exist as solute and not as solvent, EPR experiments provide us fruitful information only on the solutes and their environments can be obtained. The third reason that the spectroscopic sensitivity of EPR is reasonably high. If solute concentration in is high, the solute-solute interaction effects on the EPR spectra and rotational diffusion may not be evaluated correctly. When rotational the diffusion of D_2O and C_6D_6 in RTILs were examined by NMR, the concentration for D_2O and C_6D_6 was 50 mM and 20 mM, respectively.[24] On the other hand, the concentration of nitroxide solute, which is lower than 2 mM is enough to evaluate rotational diffusion by the EPR method. Therefore, the rotational diffusion of solutes in solvents can be evaluated more correctly by EPR.

(1.4.2) EPR study on picosecond region rotational correlation times of solutes in molecular solvents

The EPR method has been used as a tool to study the diffusion dynamics of solutes for a long time. Many papers have reported τ_R values for paramagnetic solutes in

molecular solvents determined by the EPR method.[41-43] Angerman *et al*. determined the τ_R values of vanadyl complexes in various solvents,[41] which accord well with those calculated by SED equation. For example, the rotational correlation time, τ_R^{obs}, of vanadyl perchlorate in water is determined to be 48 ps by the EPR method, which agrees well with a value of 53 ps calculated by SED equation. In this way, the rotational correlation times of paramagnetic solutes in picoseconds have been determined by using EPR spectroscopy.

(1.5) Goal and outline of the present thesis

The goal of the present thesis is to understand the rotational diffusion of smaller-sized solute in RTILs. Chart 1.1 shows pattern images of classified size relation between solute and solvent molecules for the purpose to understand rotational diffusion. The volume of coumarin 153 is 243 $Å^3$, which is larger than that of methanol (36 $Å^3$) and $BmimBF_4$ (213 $Å^3$). The volume of PADS which is used as solute in the present study is 110 $Å^3$, which is less than those of $BmimBF_4$ and the other RTILs. Rotational correlation times (τ_R^{obs}'s) of smaller-sized solutes dissolved in RTILs are derived by the aids of EPR spectroscopy and the resultant values are compared with those calculated by hydrodynamic theory (τ_R^{calc}'s).

The outlines of the subsequent chapters in the present thesis are described below.

In Chapter 2, the experimental procedures employed are described. First, the sample preparation and the EPR method used to determine rotational correlation times

experimentally are explained. Secondly, the methods of viscosity measurement and quantum chemical calculation, which are required as parameters to calculate rotational correlation times with hydrodynamic theory, are explained.

In Chapter 3, proxyl radicals which have been used as spin probe to evaluate rotational correlation times by the EPR method in molecular solvents widely, are used as solutes in RTILs. For the proxyl radicals whose shape is near sphere, CProxyH and $CProxyl^-$ is selected. The dependence of rotational correlation times for the CProxyH and $CProxyl^-$ in RTILs on (η/T) are examined by the EPR methods and compared with the estimations calculated by Stokes-Einstein-Debye (SED) equation. The difference of rotational diffusion for sphere shape solutes in RTILs between the results determined experimentally and those calculated by hydrodynamic theory is discussed.

In Chapter 4, the rotation motion and solvation of PADS nitroxide radical whose size is smaller than that of ion pair for the RTILs, are examined in various RTILs. Because the shape of PADS is prolate top, the anisotropic rotation can be examined. By analyzing the EPR spectra, the hyperfine coupling constant (A), the temperature-dependent anisotropic rotational correlation times ($\tau_{//}$ and $\tau_{\perp}$), and the rotational anisotropy (N) defined as $\tau_{\perp}/\tau_{//}$ are determined. By comparing the results of A and N values in RTILs with those in organic solvent, *N*-methylimidazole, interaction between PADS and RTILs is discussed. Based on comparing experimental values of $\tau_{//}$ and $\tau_{\perp}$ with those calculated by hydrodynamic theory with stick and slip boundary condition in various RTILs, effect of RTIL components on rotational diffusion of small

size solute is discussed.

In Chapter 5, the effect of solute size and shape on rotation diffusion in RTILs is examined. The ratios of τ_R^{obs} values for nitroxide radicals, whose shape is pseudo-sphere, and rotational correlation times calculated by hydrodynamic theory with slip boundary condition, τ_R^{slip}, are determined. Besides, a nitroxide radical, whose shape is non-sphere and ellipse, is introduced and the $\tau_R^{obs}/\tau_R^{slip}$ values are determined. By comparing the results of nitorxides, the effect of solute size and shape on its rotation motion in RTILs is discussed.

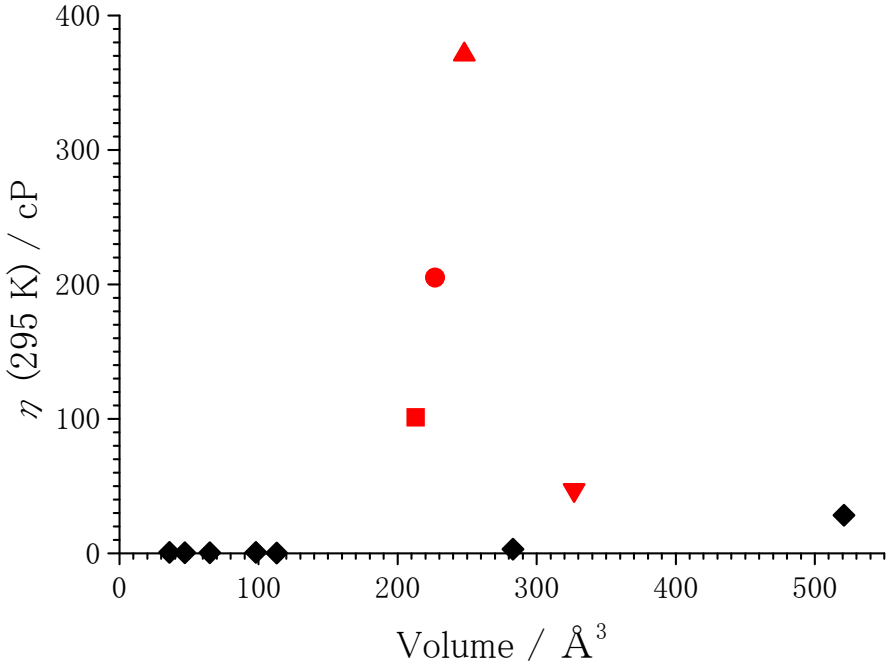

Figure 1.1: Plots of viscosity η against volume. The viscosities are the values at 295 K. The volumes are calculated by DFT calculations. Red and black colours represent Bmim cation based RTILs and traditional molecular solvents, respectively. The symbols of square, circle, triangle and upturned triangle represent RTILs coupled with BF_4, CH_3OSO_3, PF_6 and Tf_2N[12] anions, respectively. The data of traditional molecular solvents were quoted from ref 20.

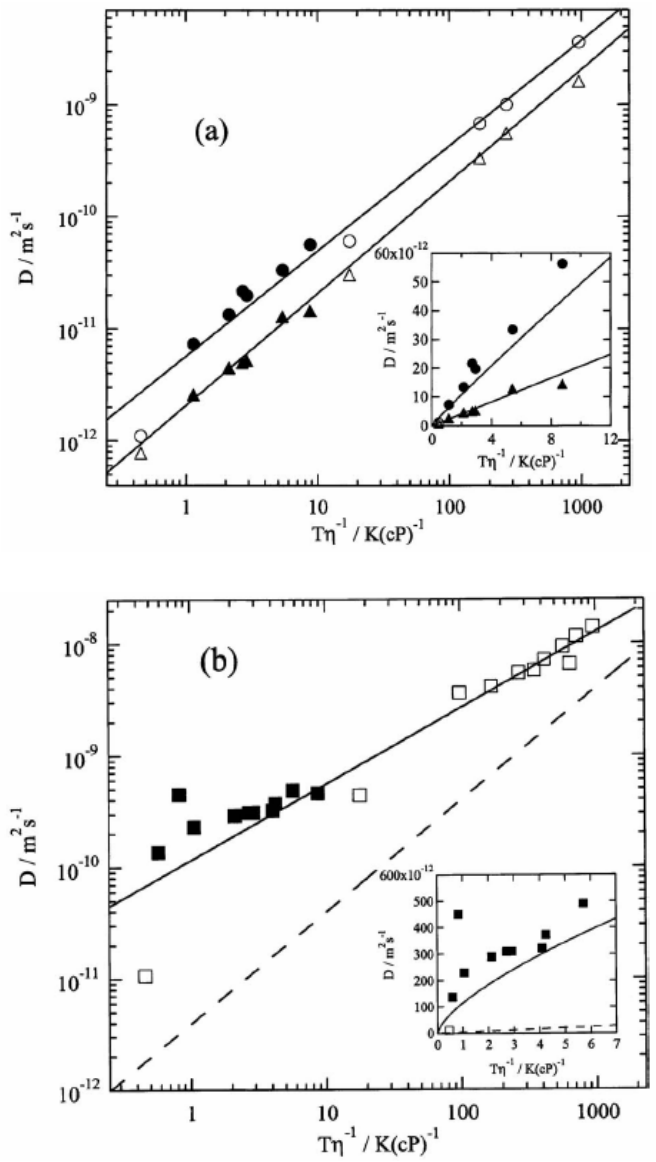

Figure 1.2: Plots of diffusion constant of (a) BP and BPK and (b) monoxide in various solvents against $T\ \eta^{-1}$. The circles, triangles and squares represent BP, BPK and monoxide, respectively. The open and closed symbols represent the ones in molecular solvents and in RTILs, respectively. The solid lines were obtained by least-squares fittings. The broken line in (b) represents the prediction from the SE equation. (Taken from ref17.)

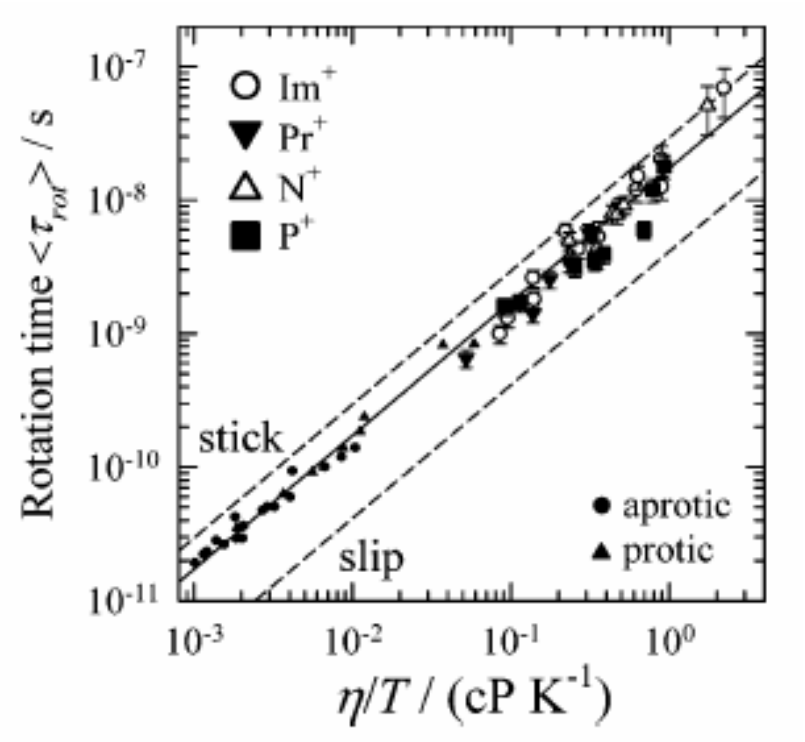

Figure 1.3: Rotational correlation times of coumarin 153 in dipolar solvents (small symbols) and RTILs (larger symbols with error bars) at room temperature plotted against η/T. The solid line shows the best fit of the dipolar liquid data. The dashed lines show the predictions of hydrodynamic calculations using stick and slip boundary conditions. (Taken from ref 31.)

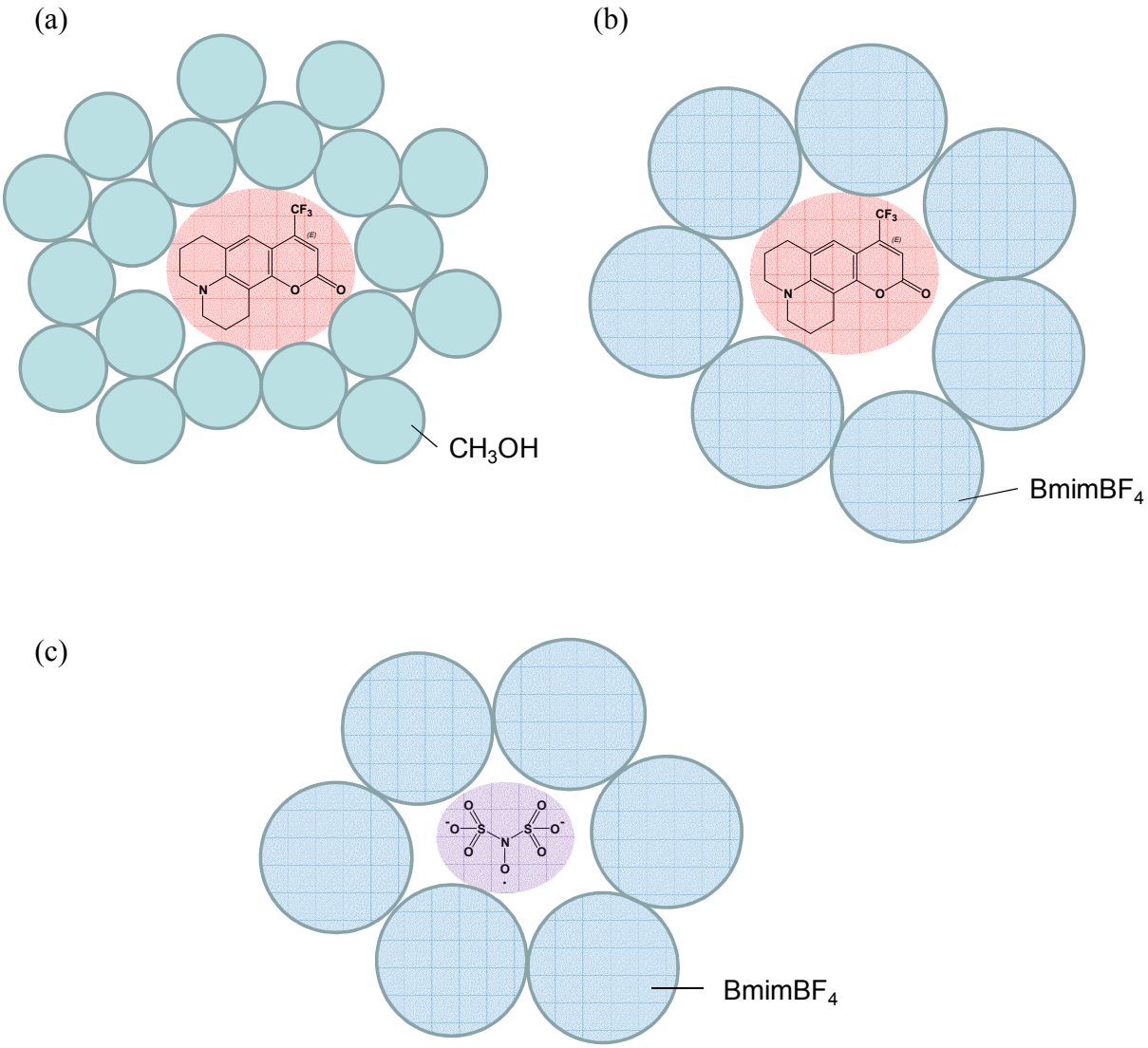

Chart 1.1: Pattern images for classified size relation between (a) coumarin 153 and methanol, (b) coumarin 153 and $BmimBF_4$ and (c) PADS and $BmimBF_4$.

Reference and notes of Chapter 1

(1) Wilkes, J. S.; Zaworotko, M. J. *J. Chem. Soc. Chem. Commun*. **1992**, 965.

(2) Welton, T. *Chem. Rev*. **1999**, *99*, 2071.

(3) Huddleston, J. G.; Willauer, H. D.; Swatloski, R. P.; Visser, A. E.; Rogers, R. D. *Chem. Commun*. **1998**, 1765.

(4) Kitazume, T.; Kasai, K. *Green Chem*. **2001**, *3*, 30.

(5) Hayashi, S.; Hamaguchi, H. *Chem. Lett*. **2004**, *33*, 1590.

(6) Yoshida, Y.; Tanaka, H.; Saito, G. *Chem. Lett*. **2007**, *36*, 1096.

(7) Miyake, Y.; Hidemori, T.; Akai, N.; Kawai, A.; Shibuya, K.; Koguchi, S.; Kitazume, T. *Chem. Lett*. **2009**, *38*, 124.

(8) Yoshida, Y.; Saito, G. *Phys. Chem. Chem. Phys*. **2010**, *12*, 1675.

(9) Asaka, T.; Akai, N.; Kawai, A.; Shibuya, K. *J. Photochem. Photobiol. A* **2010**, *209*, 12.

(10) Kawai, A.; Kawamori, D.; Monji, T.; Asaka, T.; Akai, N.; Shibuya, K. *Chem. Lett*. **2010**, *39*, 230.

(11) Tamura, H.; Shinohara, Y.; Arai, T. *Chem. Lett*. **2010**, *39*, 240.

(12) Bmim; 1-butyl-3-methylimidazolium, Tf_2N; bis(trifluoromethanesulfonyl)amide

(13) Muldoon, M. J.; McLean, A. J.; Gordon, C. M.; Dunkin, I. R. *Chem. Commun*. **2001**, 2364.

(14) Skrzypczak, A.; Neta, P. *J. Phys. Chem. A* **2003**, *107*, 7800.

(15) Paul, A.; Samanta, A. *J. Phys. Chem. B* **2007**, *111*, 1957.

(16) Morgan, D.; Ferguson, L.; Scovazzo, P. *Ind. Eng. Chem. Res*. **2005**, *44*, 4815.

(17) Nishiyama, Y.; Fukuda, M.; Terazima, M.; Kimura, Y. *J. Chem. Phys.* **2008**, *128*, 164514.

(18) Atherton, N. M. *Principles of Electron Spin Resonance*; Ellis Harwood, Chichester, 1993; Chap.9.

(19) Boere, R. T.; Kidd, R. G. *Rotational Correlation Times in Nuclear Magnetic Relaxation*.

(20) Horng, M.-L.; Gardecki, J. A.; Maroncelli, M. *J. Phys. Chem. A* **1997**, *101*, 1030.

(21) Mali, K. S.; Dutt, G. B.; Mukherjee, T. *J. Chem. Phys.* **2008**, *128*, 054504.

(22) Khara, D. C.; Samanta, A. *Phys. Chem. Chem. Phys*. **2010**, *12*, 7671.

(23) Fruchey, K.; Fayer, M. D. *J. Phys. Chem. B* **2010**, *114*, 2840.

(24) Yasaka, Y.; Wakai, C.; Matsubayashi, N.; Nakahara, M. *J. Chem. Phys*. **2007**, *127*, 104506.

(25) Dutt, G. B. *J. Phys. Chem. B* **2010**, *114*, 8971.

(26) Mali, K. S.; Dutt, G. B.; Mukherjee, T. *J. Chem. Phys*. **2005**, *123*, 174504.

(27) Ito, N.; Arzhantsev, S.; Maroncelli, M. *Chem. Phys. Lett*. **2004**, *396*, 83.

(28) Seth, D.; Sarkar, S.; Sarkar, N. *J. Phys. Chem. B* **2008**, *112*, 2629.

(29) Paul, A.; Samanta, A. *J. Phys. Chem. B* **2007**, *111*, 4724.

(30) Iwata, K.; Kakita, M.; Hamaguchi, H. *J. Phys. Chem. B* **2007**, *111*, 4914.

(31) Jin, H.; Baker, G.; Arzhantsev, S.; Dong, J.; Maroncelli, M. *J. Phys. Chem. B* **2007**, *111*, 7291.

(32) Ito, N.; Arzhantsev, S.; Heitz, M.; Maroncelli, M. *J. Phys. Chem. B* **2004**, *108*, 5771.

(33) Funston, A. M.; Fadeeva, T. A.; Wishart, J. F.; Castner, E. W., Jr. *J. Phys. Chem. B* **2007**, *111*, 4963.

(34) Shim, Y.; Jeong, D.; Choi, M. Y.; Kim, H. J. *J. Chem. Phys*. **2006**, *125*, 061102.

(35) Noel, M. A. M.; Allendoerfer, R. D.; Osteryoung, R. A. *J. Phys. Chem*. **1992**, *96*, 2391.

(36) Evans, R. G.; Wain, A. J.; Hardacre, C.; Compton, R. G. *Chem. Phys. Chem*. **2005**, *6*, 1035.

(37) Kawai, A.; Hidemori, T.; Shibuya, K. *Mol. Phys*. **2006**, *104*, 1573.

(38) Uchida, Y.; Oki, S.; Tamura, R.; Sakaguchi, T.; Suzuki, K.; Ishibashi, K.; Yamauchi, J. *J. Mater. Chem*. **2009**, *19*, 6877.

(39) Strehmel, V.; Rexhausen, H.; Strauch, P. *Phys. Chem. Chem. Phys*. **2010**, *12*, 1933.

(40) Dahl, K.; Sando, G. M.; Fox, D. M.; Sutto, T. E.; Owrutsky, J. C. *J. Chem. Phys*. **2005**, *123*, 084504.

(41) Stone, T. J.; Buckman, T.; Nordio, P.L.; McConnell, H. M. *Proc. Natl. Acad. Sci. USA* **1965**, *54*, 1010.

(42) Angerman, N. S.; Jordan, R. B. *J. Chem. Phys.* **1971**, *33*, 1094.

(43) Andreozzi, L.; Schino, A. D.; Giordano, M.; Lepori, D. *Europhys. Lett.* **1997**, *38*, 669.

Chapter 2. Experimental

(2.1) Sample preparations

Properties of RTILs significantly depend on impurities. Especially, shear viscosity remarkably changes as a function of water content. Rotational correlation times of solutes in RTILs are sensitive to viscosity and thus depend on the concentration of impurity, in particular, water content of RTIL. Therefore, gases and water impurities dissolved in RTIL samples were evacuated under vacuum for 3 days before EPR spectral measurements. After the evacuation procedure, the solution was pipetted into a quartz EPR cell with 5 or 2.6 mm diameter. The cells were connected to silica sample tubes on a vacuum line and then sealed after the evacuation of dissolved gases. Concentration of the samples was adjusted to be less than 2 mM to suppress line broadening in EPR spectra by exchange or dipolar interactions between the solutes. The effects of solvent-solute interaction on rotation are selectively evaluated by checking EPR spectra of well-diluted solutions in the present study.

Impurity water amount in samples was measured with Karl-Fisher measurement of moisture titrator (MKC-610, KYOTO ELECTRONICS). Moisture contents for each sample are summarized in Table 2.1.

(2.2) EPR Measurements

EPR spectra were recorded by an X-band EPR spectrometer (ELEXIS 580E, Bruker) with a rectangle cavity resonator of TE_{102} mode. All EPR experiments

employed a microwave power of 0.6 mW and modulation width of 0.1 G or 0.2 G. The magnetic field was calibrated by a tesla meter (ER036TM, Bruker). The temperature of samples in the EPR cavity was controlled by a temperature controller (ER4131VT, Bruker) from 240 to 330 K. The equipment for EPR measurement is described in Chart 2.1.

(2.3) Viscosity measurements

Viscosity of solvent is important physicochemical property for evaluation of τ_R by hydrodynamic equations. Viscosity of solvent was measured by a rotational viscometer (DV-Ⅱ+Pro, BROOKFIELD) with cones and plate geometry. Temperature of solvent in the viscometer was varied from 293 to 330 K by temperature controller (UA-100, EYELA). Figure 2.1 shows measured shear viscosity (η) vs temperature (T) plots of BmimPF$_6$. The η-T plot is known to follow an empirical equation,

$$\eta(\boldsymbol{T}) = \boldsymbol{a} + \boldsymbol{b}\exp\left(-\frac{\boldsymbol{T}-\boldsymbol{T}_0}{\boldsymbol{c}}\right) \qquad (2.1)$$

This equation was applied to fit the present experimental data to determine parameters, a b, c and T_0. The data on viscosities of the other RTILs were also measured and fitted by the equation. Table 2.2 summarizes the parameters of the equation for each sample. Some viscosity values at low temperature, which were not measured by the viscometer, were evaluated by eq. 2.1 with these parameters.

(2.4) Quantum chemical calculation

Volumes of both solvent and solute molecules are necessary to calculate rotational correlation times by hydrodynamic equation. To determine the volumes, density functional theory (DFT) calculation was performed by using the Gaussian 03 program[1] for all samples examined in this study. Molecular volumes were derived from B3LYP/6-31(d, p) level calculations.[2]

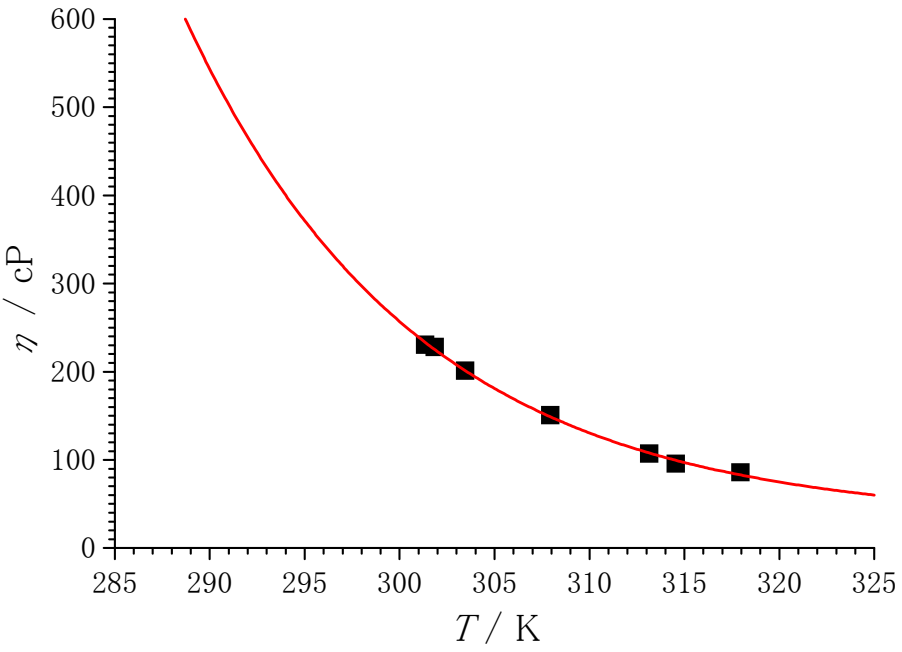

Figure 2.1: Experimental η-T plot and its best-fitted curve for $BmimPF_6$ assuming eq.2.1.

Table 2.1: Water contents of solvents

solvent	water content / %
$PP_{13}Tf_2N$	< 0.001
$Py_{13}Tf_2N$	< 0.001
$DemeTf_2N$	< 0.01
$P_{146666}Tf_2N$	0.002
$Py_{14}Tf_2N$	0.055
$BmimPF_6$	0.073
$N_{3111}Tf_2N$	0.098
$EmimBF_4$	0.15
$BmimCH_3OSO_3$	0.18
$BmimBF_4$	< 0.43
$DemeBF_4$	0.58
$EmimEtOSO_3$	0.60
N-methylimidazole	< 0.001

Table 2.2: Best-fitted parameters in the empirical equation for temperature dependent solvent viscosity [a)]

solvent	a / cP	b / cP	c / K	T_0 / K
$DemeBF_4$	-10.43	442.78	16.81	294.55
$EmimBF_4$	-8.14	35.88	45.61	299.35
$BmimBF_4$	0.65	4.03	15.36	298.15
$N_{3111}Tf_2N$	3.36	44.45	21.72	299.75
$BmimTf_2N$	4.77	35.62	23.49	298.75
$EmimC_2H_5OSO_3$	6.69	43.48	19.54	299.65
$PP_{13}Tf_2N$	8.63	49.84	19.23	298.35
$DemeTf_2N$	9.23	77.80	17.90	292.95
$Py_{14}Tf_2N$	12.25	65.85	16.33	298.05
$Py_{13}Tf_2N$	13.75	101.83	16.47	300.35
$BmimCH_3OSO_3$	14.76	140.11	14.67	299.45
$BmimPF_6$	30.87	202.42	12.22	301.35
N-methylimidazole	0.18	1.49	43.19	293.15

a) equation (2.1)

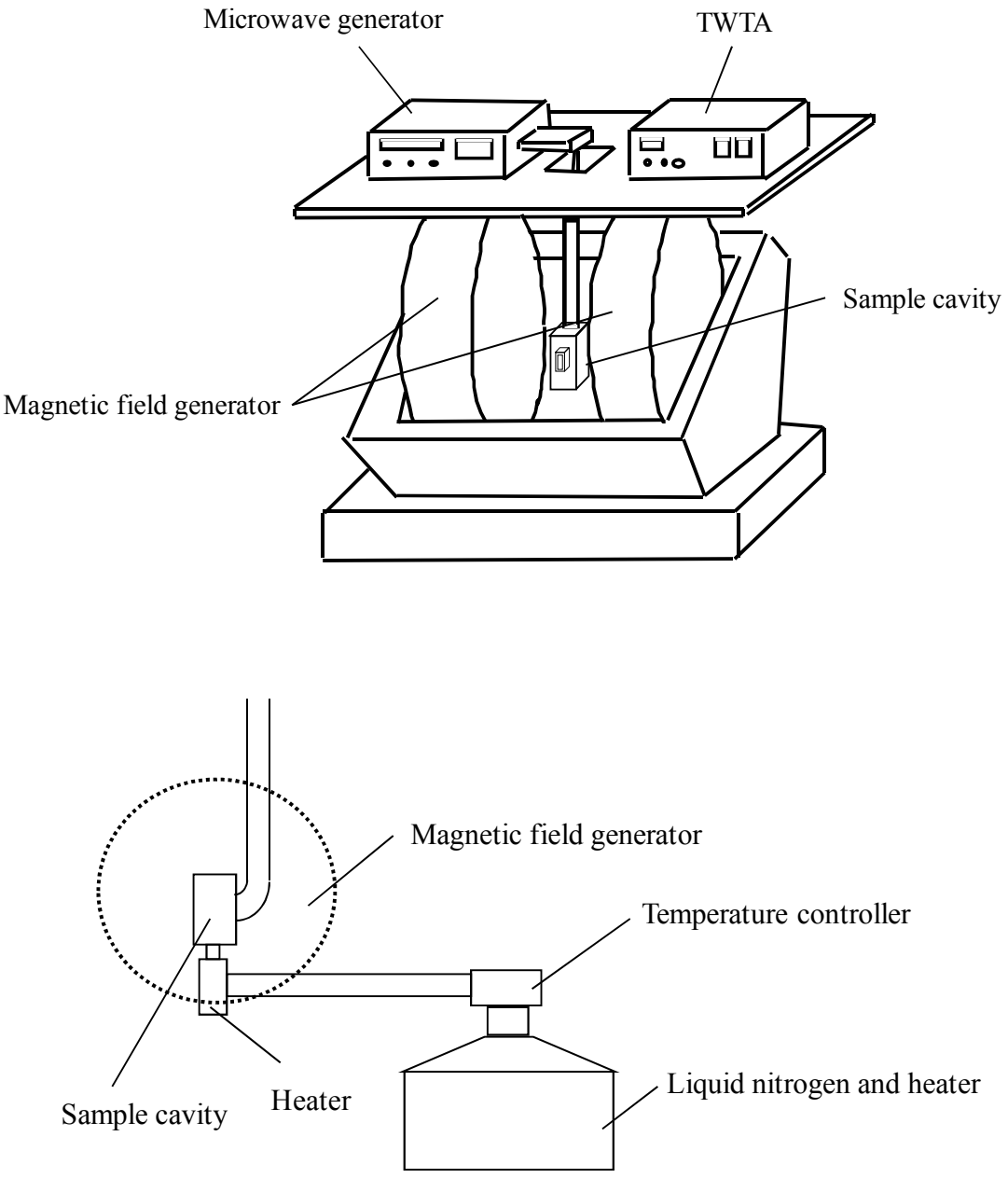

Chart 2.1: Equipment for EPR measurement and temperature controller.

References of Chapter 2

(1) Freisch, M. J.; Trucks, G. W.; Schlegel, H. B.; Scuseria, G. E.; Robb, M. A.; Cheeseman, J. R.; Montgomery, J. A., Jr.; Vreven, T.; Kudin, K. N.; Burant, J. C.; Milliam, J. M.; Iyengar, S. S.; Tomasi, J.; Barone, V.; Mennucci, B.; Cossi, M.; Scalmani, G.; Rega, N.; Petersson, G. A.; Nakatsuji, H.; Hada, M.; Ehara, M.; Toyota, K.; Fukuda, R.; Hasegawa, J.; Ishida, M.; Nakajima, T.; Honda, Y.; Kitano, O.; Nakai, H.; Klene, M.; Li, X.; Knox, J. E.; Hratchian, H. P.; Cross, J. B.; Bakken, V.; Adamo, C.; Jaramillo, J.; Gomperts, R.; Stratmann, R. E.; Yazyev, O.; Austin, A. J.; Cammi, R.; Pomelli, C.; Ochterski, J. W.; Ayala, P. Y.; Morokuma, K.; Voth, G. A.; Salvador, P.; Dannenberg, J. J.; Zakrzewski, V. G.; Dapprich, S.; Daniels, A. D.; Strain, M. C.; Farkas, O.; Malick, D. K.; Rabuck, A. D.; Raghavachari, K.; Foresman, J. B.; Ortiz, J. V.; Cui, Q.; Baboul, A. G.; Clifford, S.; Cioslowski, J.; Stefanov, B. B.; Liu, G.; Liashenko, A.; Piskorz, P.; Komaromi, I.; Martin, R. L.; Fox, D. J.; Keith, T.; Al-Laham, M. A.; Peng, C. Y.; Nanayakkara, A.; Challacombe, M.; Gill, P. M. W.; Johnson, B.; Chen, W.; Wong, M. W.; Gonzalez, C.; Pople, J. A. *Gaussian 03, Revision D.02*; Gaussian, Inc.: Wallingford, CT, 2004.

(2) Jin, H.; O'Hare, B.; Dong, J.; Arzhantsev, S.; Baker, G. A.; Wishart, J. F.; Maroncelli, M. *J. Phys. Chem. B* **2008**, *112*, 81.

Chapter 3. Breakdown of Stokes-Einstein-Debye theory for rotational diffusion of proxyl in $BmimPF_6$ and $BmimBF_4$

(3.1) Introduction

Nitroxide radicals have been used as solutes and rotation motion of solutes in various solvents has been examined by analyzing EPR spectra for the radicals.[1-5] EPR spectra for nitroxide radicals are dominated by very simple three peaks due to nuclear spin of ^{14}N atom and both linewidth and intensity pattern depend on rotational diffusion rate of nitroxide radicals. The EPR spectra whose lineshape is Lorentzian have been examined in detail.[6] In this study, proxyl radical which is one of nitroxide radicals was used as solute in RTILs and, by analyzing EPR spectra, rotational correlation times, τ_R^{obs} for the proxyl radicals in RTILs were determined. The theoretical rotational correlation time, τ_R^{calc} values are also obtained by Stokes-Einstein-Debye (SED) hydrodynamic equation which has been widely used to evaluate rotation diffusion of solute in molecular solvents. The SED hydrodynamic equation is formulated for isotropic rotational correlation time and described as,

$$\tau_R^{calc} = \frac{V_p \eta}{k_B T} \qquad (3.1)$$

where V_p is volume of solute, η is shear viscosity, k_B is Boltzmann constant and T is temperature. If there is difference between τ_R^{obs} and τ_R^{calc} values, environment around solute may be different from that expected by SED hydrodynamic theory. To evaluate the discrepancy between τ_R^{obs} and τ_R^{calc} values, dependence of τ_R^{obs} value on (η/T) is

focused and the following fractional relation,

$$\tau_R^{obs} \propto \left(\frac{\eta}{T}\right)^t \qquad (3.2)$$

between τ_R^{obs} and η/T is introduced.[7] If t value is unity, τ_R^{obs} value is proportional to (η/T) which is essentially the same as SED equation, and actually, many molecular solvents, show t values of almost unity.[7-9] If t value is not unity, SED equation should be modified to reflect the individual solute environment.

In this chapter, the τ_R^{obs} values of proxyl radicals, CProxyl$^-$ and CProxylH whose structures are shown in Chart 3.1 were determined in RTILs at various temperatures and the t values were evaluated accurately. The t values for CProxylH and CProxyl$^-$ in $BmimPF_6$ and $BmimBF_4$ were compared with those in molecular solvents, and discussed non-SED behavior of rotational diffusion of solutes in RTILs.

(3.2) Experimental

CProxylH used as solute was purchased from Tokyo Kasei. $BmimBF_4$ and $BmimPF_6$ were supplied by Kanto Chemical. BmimCProxyl was synthesized according to the reaction pathways shown in Scheme 3.1. CProxylH and Ag_2O in distilled water were stirred at 298 K for 24 h and the resultant aqueous solution was filtered to remove dissolved Ag_2O. BmimBr was added to the remaining aqueous solution until AgBr precipitation was not observed. After filtration, the remaining solution was heated at 310 K under vacuum to remove water, and a yellow liquid containing BmimCProxyl

was produced. The crude residue was dissolved in acetonitrile to remove remaining silver compounds. After the evaporation of acetonitrile, pure BmimCProxyl liquid was obtained. BmimCProxyl was identified with IR and NMR spectrometers. For IR measurement, neat RTIL samples were put in a cell with CaF_2 or KBr windows and the spectra were measured by a FT/IR - 4100 spectrometer (JASCO). The NMR spectra were measured by a 300 MHz NMR spectrometer (JEOL). The IR and ^{1}H-NMR spectra showed the product to be composed of $Bmim^+$ and $CProxyl^-$.

For EPR measurements, diluted solutions of radicals in RTILs were prepared with concentration of ca. 2 mM and were dried with the method explained in Chapter 2. A small amount of the samples was introduced into a quartz EPR sample cell with 5 mm inner diameter. The cells were connected to a vacuum line and then sealed after evacuation of dissolved oxygen.

(3.3) Results and Discussion

(3.3.1) Determination of rotational correlation time τ_R

Figure 3.1 shows an EPR spectrum of CProxylH radical in $BmimPF_6$. The spectrum is composed of triplet hyperfine lines due to ^{14}N nuclear spin. The similar spectrum was obtained for $CProxy^-$ in $BmimBF_4$. In these spectra, intensities of hyperfine lines are not equivalent, which indicates that anisotropic terms in hyperfine and *g* tensors are not negligible. This asymmetric intensity pattern is related to how the molecular rotation of radicals averages out these anisotropic terms, namely, fast rotation gives only

isotropic terms whereas slow rotation leaves anisotropic terms as well as isotropic interactions. According to Kivelson's theory,[6] rotational correlation time, τ_R^{obs} of rapidly rotating nitroxide radicals can be described by the equation

$$\tau_R^{obs} = 6.0\times10^{-10}\left\{\sqrt{\frac{h_0}{h_{+1}}}+\sqrt{\frac{h_0}{h_{-1}}}-2\right\}\Delta H(0)\,. \qquad (3.3)$$

The position of h_{+1}, h_0, h_{-1} and $\Delta H(0)$ were referred to Figure 3.1. This theory can be used for nitroxide radicals which satisfies two conditions as described below. One condition is that spectral shape of triplet hyperfine lines is Lorentzian lineshape. Since proxyl radicals have several hydrogen atoms, inhomogeneous broadening due to nuclear spin of H atom may occur, and which leads to non-Lorentzian spectral lineshape. The other is that h_0 is larger than h_{+1}. If h_0 is smaller than h_{+1}, rotation of the nitroxide radical may be anisotropic and the present Kivelson's theory which is for isotropic rotation is not applicable. The EPR spectra of CProxylH in $BmimPF_6$ and $CProxyl^-$ in $BmimBF_4$ satisfy both the two conditions. Therefore, analysis on these two samples was safely performed and the τ_R^{obs} values were determined by eq (3.3). The τ_R^{obs} values were compared with τ_R^{calc} values calculated by SED hydrodynamic equation as described in eq (3.1). The V_p values of proxyl radicals were calculated by density for the proxyl radicals. The τ_R^{obs} values for CProxylH in $BmimPF_6$ and $CProxyl^-$ in $BmimBF_4$ at 298 K are 1.5 ns and 1.2 ns, respectively, and they are shorter than τ_R^{calc} values which are 16.4 ns and 5.0 ns, respectively.

(3.3.2) Arrhenius parameters for rotation in RTILs

In order to obtain more detailed information on rotation dynamics in RTILs, the τ_R value was measured at various temperatures and Arrhenius parameters were determined from τ_R^{obs} vs. $1/T$ plots as shown in Figure 3.2. The activation energy E_a^{obs} determined for CProxylH in $BmimPF_6$ and $CProxyl^-$ in $BmimBF_4$ are summarized in Table 3.1. By using SED equation, τ_R value was calculated for various temperature and E_a^{calc} values are determined as summarized in Table 3.1. By comparing E_a^{obs} and E_a^{calc} values, one may recognize that measured E_a^{obs} values were by 8 - 15 kJ/mol lower than the calculated ones. These results lead the conclusion that the SED equation does not hold for proxyls in these solvents and proxyl radicals rotates more easily than expected by SED equation.

(3.3.3) Rotational diffusion evaluated by fractional SED equation

In the case SED equation does not hold, the experimental results of τ_R^{obs} were examined by fractional SED equation defined in eq (3.2). Figure 3.3 shows plots of τ_R^{obs} against (η/T) for two samples. The plots show linear dependence and thus the t values were determined as the slopes of the lines. It is interesting to note that the SED equation should be modified by introducing fractional parameter t of about 0.7 for these two samples.

In order to find a general trend in the t-η relation, we plotted the t-parameter vs. log (viscosity) as shown in Figure 3.4. In addition to the present data, t-parameters for

rotation of nitroxide radicals obtained from the literature[7-9] were also plotted. In these literature works, rotational motions were studied in organic solvents, toluene, EtOH (= ethanol), OTP (= *o*-terphenyl) and SALOL (= phenyl-salicylate). It is interesting that the *t*-parameters in organic solvents remains essentially a unity in a wide range of viscosity, $\eta \leqq 435$ cP, which indicates that the rotational motion in organic solvents follows the SED equation regardless of the η value. On the other hand, the situation seems different in RTILs as clearly shown in Figure 3.4.

As *t* value is less than unity, solutes slip in these solvents during rotational motion as hydrodynamic model is valid. A similar conclusion has been reported for the rotation of TEMPO in supercooled organic liquids. The *t*-parameters in the fractional SED equation have been determined to be 0.28 for OTP (< 298 K)[7] and 0.46 for SALOL (< 278 K)[8] in which non-thermal dynamics are considered. $BmimPF_6$ and $BmimBF_4$ are certainly different from supercooled solvents and different rotation dynamics are expected to occur.

The above-mentioned observation may indicate that solutes rotate more easily than expected by the SED equation based on shear viscosity of solvent in $BmimPF_6$, and in $BmimBF_4$.

(3.4) Conclusion

By using proxyl radicals as EPR spectroscopy probe, the rotational dynamics of the solutes in RTILs was examined. Rotational correlation times of CProxylH in $BmimPF_6$

and CProxyl$^-$ in $BmimBF_4$ were successfully determined and compared with those calculated by SED equation. Activation energies for rotational correlation times determined experimentally are lower than those calculated by SED equation. This means CProxylH in $BmimPF_6$ and CProxyl$^-$ in $BmimBF_4$ rotate more easily than expected by SED equation.

The dependence of rotational correlation times on (η/T) was evaluated for CProxylH in $BmimPF_6$ and CProxyl$^-$ in $BmimBF_4$. This low t value may indicate that solutes rotate more easily than expected by the SED equation based on shear viscosity of solvent in $BmimPF_6$, and in $BmimBF_4$. The plots were well fitted by $\tau \propto (\eta/T)^t$ relation with t value of about 0.7.

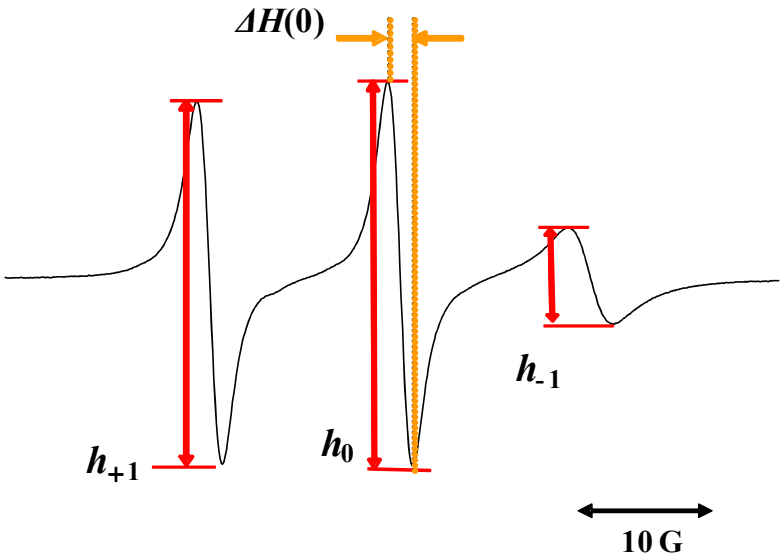

Figure 3.1: EPR spectrum of CProxylH in $BmimPF_6$ at 303 K.

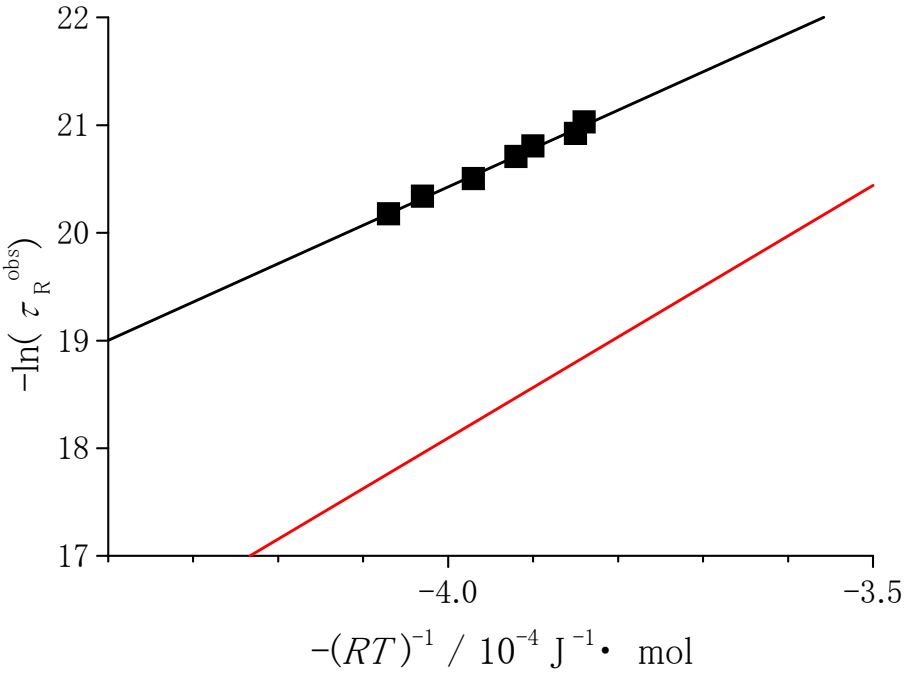

Figure 3.2: Rectangular data points are ($1/\tau_R^{obs}$) vs (-1/*RT*) plots for CProxylH in $BmimPF_6$. The black line was obtained by the least-squares fitting procedure. The red line shows the simulation based on SED hydrodynamic theory.

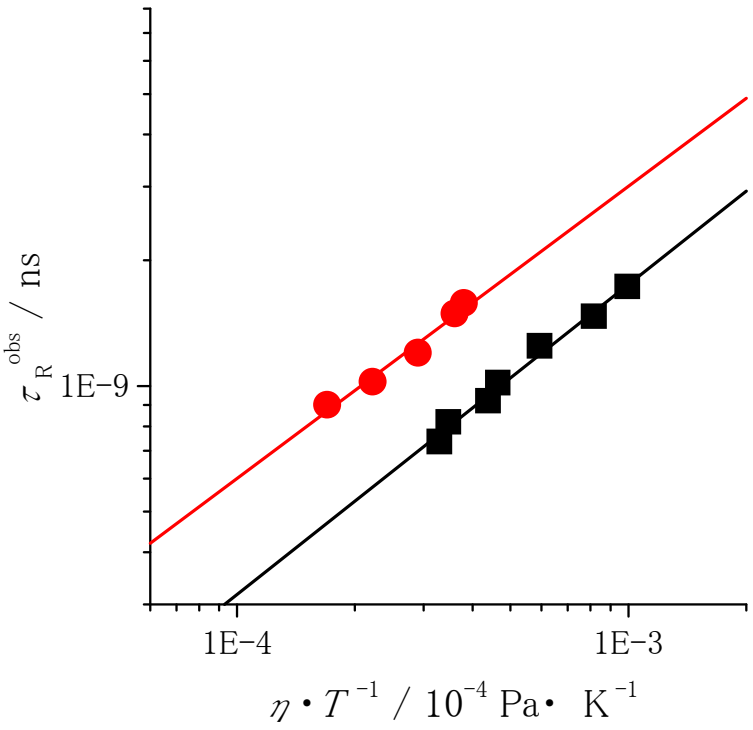

Figure 3.3: τ_R^{obs} vs (η/T) plots for CProxyl$^-$ in $BmimBF_4$ (●) and CProxylH in $BmimPF_6$ (■). The solid lines are obtained by the least square fitting procedure assuming $\tau_R^{obs} \propto (\eta/T)^t$ relation.

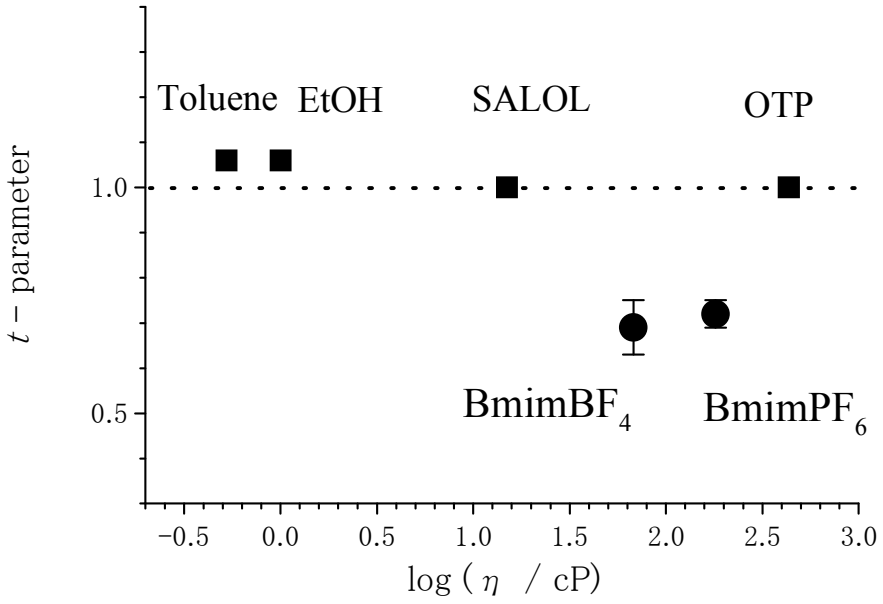

Figure 3.4: Parameter t – log η (at 303 K) plots.

Table 3.1: Activation energies (kJ mol^{-1}) for rotational diffusion motion derived from rotational correlation times.

	E_a^{obs}	E_a^{calc}
CProxylH in $BmimPF_6$	34.2 ± 1.2	46.9 ± 0.7
$CProxyl^-$ in $BmimBF_4$	27.6 ± 2.3	41.3 ± 0.2

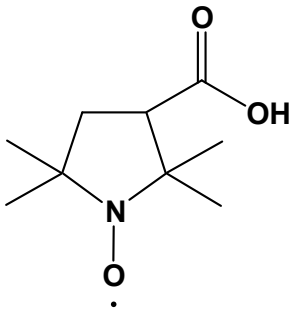

(CProxylH)

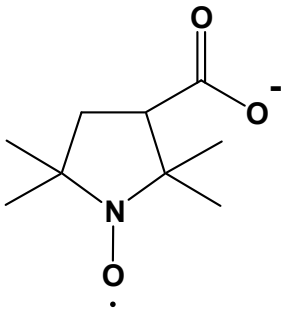

(CProxyl$^-$)

Chart 3.1: Structure of proxyl radicals used as solute

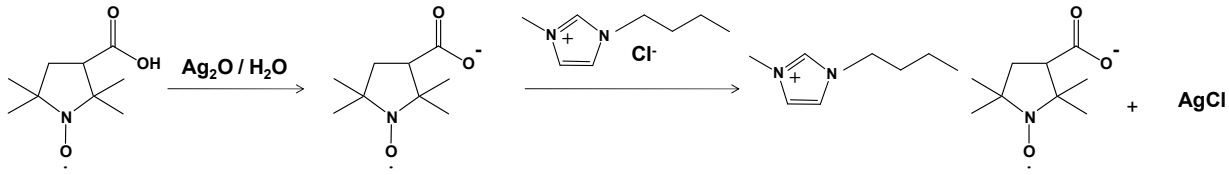

Scheme 3.1: Synthesis of BmimCProxyl

References of Chapter 3

(1) Polnaszek, C. F.; Schreier, S.; Butler, K. W.; Smith, I. C. P. *J. Am. Chem. Soc.* **1978**, *100*, 8223.

(2) Schreier, S.; Polnaszek, C. F.; Smith, I. C. P. *Biochim. Biophys. Acta*. **1978**, *515*, 375.

(3) Belton, P. S.; Sutcliffe, L. H.; Gillies, D. G.; Wu, X.; Smirnov, A. I. *Magn. Reson. Chem*. **1999**, *37*, 36.

(4) Pilar, J.; Labsky, J.; Marek, A.; Budil, D. E.; Earle, K. A.; Freed, J. H. *Macromolecules* **2000**, *33*, 4438.

(5) Stone, T. J.; Buckman, T.; Nordio, P. L.; McConnell, H. M. *Proc. Natl. Acad. Sci. USA* **1965**, *54*, 1010.

(6) Kivelson, D *J. Chem. Phys.* **1960**, *33*, 1094.

(7) Andreozzi, L.; Di Schino, A.; Giordano, M.; Lepori, D. *Europhys. Lett*. **1997**, *38*, 669.

(8) Andreozzi, L.; Bagnoli, M.; Faetti, M.; Giordano, M. *J. Non-Crys. Sol*. **2002**, *303*, 262.

(9) Hwang, J. S.; Mason, R. P.; Hwang, L. P.; Freed, J. H. *J. Phys. Chem.* **1975**, *79*, 489.

Chapter 4. Anisotropic rotational diffusion of proxylamine disulfonate (PADS) nitroxide radical in RTILs

(4.1) Introduction

In Chapter 3, rotational correlation times, τ_R^{obs} of proxyl radicals whose shape is pseudo-sphere in $BmimPF_6$ and $BmimBF_4$ were measured by EPR spectroscopy. To examine difference of rotational diffusion in RTILs and molecular solvents, the τ_R^{obs} values were compared with rotational correlation times, τ_R^{calc}, calculated by Stokes-Einstein-Debye (SED) hydrodynamic equation which is simple theory for rotational motion of sphere solute and has been widely used for rotational diffusion of solutes in molecular solvent. In the result, the τ_R^{obs} values are τ_R^{calc} values and the activation energy determined by Arrhenius plots for $(1/\tau_R^{obs})$ is lower than that for $(1/\tau_R^{calc})$. The difference between τ_R^{obs} and τ_R^{calc} for (η/T) dependence is evaluated by t value defined as $\tau_R \propto (\eta/T)^t$ and the t values are about 0.7. These results suggest solutes in $BmimPF_6$ and $BmimBF_4$ rotate more easily than SED hydrodynamic theory.

To examine rotational diffusion of solutes in RTILs in more detail, this chapter focused on the anisotropic rotational motion of solute, and the solute-solvent interaction in RTILs. The peroxylamine disulfonate (PADS) nitroxide radical (Chart 4.1) was chosen as a small-sized solute molecule. The molecular volume of PADS is ~110 $Å^3$, which is smaller than well-studied fluorescent solutes such as anthracene (~175 $Å^3$), coumarin 153 (~246 $Å^3$), and peryrene (~225 $Å^3$).[1-3] The ^{14}N isotropic hyperfine coupling constant (A) and rotational anisotropy of PADS in RTILs were determined by

analyzing the EPR spectra. From the *A* values and rotational anisotropy of PADS in RTILs, solvated structures of PADS in RTILs were discussed. Based on the lineshape analysis,[4] the rotational correlation times of PADS in various RTIL solutions were determined and discussed based on hydrodynamic theory with the stick/slip boundary conditions of the solute-solvent interactions.

(4.2) Experimental

Potassium peroxylamine disulfonate (K_2PADS) and *N*-methylimidazole were purchased from Tokyo Kasei. Ionic liquid samples were supplied by Kanto Chemical except Emim$C_2H_5OSO_3$ from BASF and BmimCH_3OSO_3 from Fruka.[5] The structures of PADS and these RTILs are listed in Charts 4.1 and 4.2. RTILs were prepared as explained in Chapter 2. *N*-methylimidazole was dehydrated with molecular sieve 3A 1/16 (Kanto Chemical) for 3 days and deoxygenated by bubbling with Ar for ca. 10 min. The sample solution was filtered in order to remove undissolved solutes. The concentration of PADS was less than 2 mM.

(4.3) Results and Discussion

(4.3.1) Isotropic hyperfine coupling constant of PADS radical

Figure 4.1 shows the EPR spectra of PADS in BmimPF_6 measured at (a) 295 K and (b) 320 K. The spectra show triplet hyperfine structure due to nuclear spin (I=1) of ^{14}N. Similar spectra were obtained for PADS radical in various solvents including RTILs.

The *g* and *A* values of PADS radical were determined by analyzing these EPR spectra and the results are summarized in Table 4.1. It has been known that the *A* value of nitroxide free radicals in solution is sensitive to the polarity of solvent.[6-8] In terms of valence bond theory, two canonical structures can be drawn for nitroxide radicals as shown in Chart 4.3. The *A* value of nitroxide radicals is related to spin density on N atom and thus, depends on the charge-transfer (CT) nature of N-O group. Polar solvent stabilizes the CT canonical structure and the spin density at N atom is enhanced, which results in larger *A* value in polar solvent. PADS is classified to nitroxide radical and polarity dependence of *A* value is expected. However, there is no report on solvent effect of *A* value because PADS is not soluble in conventional solvents except water. It is noteworthy that PADS is found to be soluble well in various RTILs. Hence, we examined the *A* value of PADS against solvent polarity. $E_T(30)$ is a widely-quoted empirical parameter for polarity[9] and Table 4.1 lists the $E_T(30)$ values reported for various RTILs.[4,7,8,10-13] Figure 4.2 plots the *A* values against $E_T(30)$. As already reported, 4-amino-2,2,6,6-tetramethylpiperidine-1-oxyl (ATEMPO) radical, which is another nitroxide radical, shows a good linear correlation between *A* and $E_T(30)$ values in RTILs and in organic solvents.[8] This means interaction between the N-O group of ATEMPO and polar solvent stabilizes CT canonical structure of ATEMPO and the spin density at N atom of ATEMPO becomes high in polar solvent. On the other hand, the *A* values of PADS radical does not change against $E_T(30)$ and are essentially constant for all the solvents. This indicates negligible interaction between the N-O group of PADS and

solvents regardless of the solvent polarity. Since PADS has two sulfonyl groups with negative charge, preferentially the cations of RTIL would bind to these electron rich parts of PADS and the spin density at the N atom does not change by solvation. This feature is contrast to ATEMPO which undergoes solvation at N-O group.

(4.3.2) Anisotropic rotational motion of PADS radical

It has been known that asymmetric triplet hyperfine structure of nitroxide radicals is related to rotational correlation time, τ_R of the radicals. As seen in Figure 4.1, the EPR linewidths of PADS in $BmimPF_6$ are not identical for triplet peaks. Moreover, the linewidth measured at 295 K becomes wider than that at 320 K. This feature roughly indicates that the rotational correlation time of PADS in $BmimPF_6$ at 295 K is much longer than that at 320 K. This experimental observation suggests that information on the temperature dependence of the rotational motion of PADS radical in RTILs is obtained from the EPR spectroscopy, and the detailed EPR analysis was performed as described below.

The geometric structure of PADS radical is approximated as a prolate shape, and its unique axis lies along the SO_3-N-SO_3 pseudo-line as already treated by Freed and coworkers.[4] Chart 4.1 presents the molecular axes of PADS, where y-axis is parallel (//) to the unique axis, and the other x- and z-axes are perpendicular ($\perp$) to it. Rotational correlation times for rotational motion around the perpendicular and parallel axes are defined as $\tau_{//}$ and $\tau_{\perp}$, respectively, and were determined by analyzing the EPR spectra

recorded.

As the viscosity of the solution decreases with increasing temperature, the rotational correlation time (τ_R) of the radical becomes shorter and the anisotropies in the hyperfine coupling and *g*-tensors are effectively averaged out. In a so-called "fast-motion region" of $\tau_R \leqq 3\times10^{-9}$ s, the τ_R values can be determined via a motional narrowing theory.[46] According to this theory, the linewidths in the EPR spectra having asymmetric line broadening can be fitted to a quadratic equation with the nuclear spin quantum number, m_I, as follows.

$$\Delta H(m_I) = A + Bm_I + Cm_I^2 \qquad (4.1)$$

As far as EPR spectra show Lorentzian lineshape, parameters of *B* and *C* are calculated by the following equations

$$B = \frac{1}{2}\Delta H(0)\left(\sqrt{\frac{I_0}{I_{+1}}} - \sqrt{\frac{I_0}{I_{-1}}}\right) \qquad (4.2)$$

$$C = \frac{1}{2}\Delta H(0)\left(\sqrt{\frac{I_0}{I_{+1}}} + \sqrt{\frac{I_0}{I_{-1}}} - 2\right) \qquad (4.3)$$

where $m_I = \pm 1, 0$ for PADS radical, $\Delta H(0)$ is the linewidth of the center peak, and I_{+1}, I_0, I_{-1} are relative heights of hyperfine lines as depicted in Figure 4.1(a).[14] Figure 4.3 shows expanded views of the center peak of PADS in $BmimPF_6$ at (a) 295 K and (b) 320 K. The spectral shapes are well fitted by a Lorentzian lineshape. Since PADS does not have any hydrogen atom, no inhomogeneous broadening due to the nuclear spin of H atom occurs in each hyperfine line. This is a quite advantageous point of the present study,

where PADS radical is used instead of other nitroxide radicals containing H atoms. It was carefully checked that all the EPR spectra of PADS recorded in this study were well fitted by a Lorentzian lineshape. The linewidth of $\Delta H(0)$ and the ratios of I_0/I_{+1} and I_0/I_{-1} were obtained from the spectra, and parameters of B and C were determined at temperatures examined.

When rotational correlation times of nitoxide are in the fast-motion region and the shape of solute is approximated as a prolate top, the EPR spectral parameters, B and C, are expressed by the following equations.[4]

$$B = \frac{2}{\sqrt{3}\gamma_e}\frac{\pi}{10}\omega_0\left[g_0 A_0 \tau_{2,0}\left\{\frac{16}{3}+\frac{4}{1+\omega_0^2\tau_{2,0}^2}\right\}+2g_2 A_2 \tau_{2,\pm2}\left\{\frac{16}{3}+\frac{4}{1+\omega_0^2\tau_{2,\pm2}^2}\right\}\right] \qquad (4.4)$$

$$C = \frac{2}{\sqrt{3}\gamma_e}\frac{4\pi^2}{5}\left[{A_0}^2\tau_{2,0}\left\{\frac{8}{3}-\frac{1}{1+\omega_A^2\tau_{2,0}^2}-\frac{1}{3\left(1+\omega_0^2\tau_{2,0}^2\right)}\right\}+2{A_2}^2\tau_{2,\pm2}\left\{\frac{8}{3}-\frac{1}{1+\omega_A^2\tau_{2,\pm2}^2}-\frac{1}{3\left(1+\omega_0^2\tau_{2,\pm2}^2\right)}\right\}\right] \qquad (4.5)$$

The A_i and g_i are anisotropy of hyperfine coupling tensor and g-tensor, respectively, for i = 0 and 2 in the unit of Hertz. The $\tau_{l,m}$ is rotational correlation time for quantum numbers, l and m derived from Shrödinger equation for rotational motion which will be discussed later. The ω_0 and ω_A are Larmor frequencies of electron and nuclear spins, respectively. The γ_e is magnetogyric ratio. The A_i and g_i values for PADS are available from a literature.[4] The $\tau_{//}$ and $\tau_{\perp}$ values which are our present interest are related to $\tau_{2,0}$ and $\tau_{2,\pm2}$ by the following equations.[15]

$$\tau_{\perp} = \tau_{2,0} \qquad (4.6)$$

$$\tau_{//} = \frac{2\tau_{2,0}\tau_{2,\pm2}}{3\tau_{2,0} - \tau_{2,\pm2}} \qquad (4.7)$$

The $\tau_{2,0}$ and $\tau_{2,\pm2}$ values are calculated by introducing experimentally-determined *B* and *C* values into equations (4.4) and (4.5). Then using these $\tau_{2,0}$ and $\tau_{2,\pm2}$ values, the $\tau_{\perp}$ and $\tau_{//}$ values are derived from equations (4.6) and (4.7). For a prolate top molecule like PADS, the anisotropy of rotation, *N*, is defined as

$$N = \frac{\tau_{\perp}}{\tau_{//}} \qquad (4.8)$$

The $\tau_{\perp}$ values were plotted against $\tau_{//}$ values as shown in Figure 4.4 to determine the *N* values of PADS dissolved in various solvents. A good linear correlation between $\tau_{\perp}$ and $\tau_{//}$ is recognized for all the solvents studied here. From the slopes of the fitted lines, the rotational anisotropy of PADS was determined and the resultant values are listed in Table 4.2. The *N* values of PADS in organic solvent, *N*-methylimidazole, is nearly 2, whereas the *N* values of PADS in RTILs are 3 ~ 5. This interesting feature of solvent-depending *N* values will be discussed later by comparing experimental and theoretical *N* values.

Temperature dependence of rotational correlation times, $\tau_{\perp}$ and $\tau_{//}$, were also measured in this study and some of the experimental results are shown in Figure 4.5 for three RTIL solutions. The measured rotational rates, derived from $(\tau_{\perp})^{-1}$ and $(\tau_{//})^{-1}$, follow the Arrhenius equation and Arrhenius parameters were determined. They were summarized in Table 3.

(4.3.3) Theoretical evaluation for anisotropic rotation of PADS radical

The experimental values of rotational correlation times and rotational anisotropy determined in the proceeding section are compared with those calculated by a hydrodynamic theory for diffusional motion. The hydrodynamic theory for rotational motion is reviewed as follows. The following rotational diffusion equation

$$\frac{\partial P(\varphi,\theta,\psi)}{\partial t} = D_{\perp}\left\{\frac{1}{\sin\theta}\frac{\partial}{\partial\theta}\left(\sin\theta\frac{\partial}{\partial\theta}\right)+\frac{1}{\sin^2\theta}\frac{\partial^2}{\partial\varphi^2}-\frac{2\cos\theta}{\sin^2\theta}\frac{\partial^2}{\partial\varphi\partial\psi}+\left(\cot^2\theta+\frac{D_{//}}{D_{\perp}}\right)\frac{\partial^2}{\partial\psi^2}\right\}P(\varphi,\theta,\psi) \tag{4.9}$$

is required to be solved to calculate the values of $\tau_{\perp}$ and $\tau_{//}$ for a prolate top molecule in the liquid. Here, $D_{\perp}$ and $D_{//}$ are the principal values of the diffusion tensor, and (φ, θ, ψ) are the Euler angles.[15,16] The rotational correlation times derived from EPR spectroscopy are related to the second-rank Legendre polynomial derived from equation (4.9) and then derived as simple equation (4.10).

$$\tau_{\mathrm{i}} = \frac{1}{6D_{\mathrm{i}}}, \qquad (\mathrm{i} = // \quad \text{or} \quad \perp) \tag{4.10}$$

The $D_{//}$ and $D_{\perp}$ values of a prolate top molecule, which are characterized by effective hydrodynamic radii of $r_{//}$ and $r_{\perp}$ with a relation that $r_{//} > r_{\perp}$, are calculated by equation (4.11).[16]

$$D_{\mathrm{i}} = \frac{k_{\mathrm{B}}T}{8\pi\eta r_{//}^3\sigma_{\mathrm{i}}}, \qquad (\mathrm{i} = // \text{ or } \perp) \tag{4.11}$$

Here

$$\sigma_{//} = \left(\frac{2}{3}\right)\frac{\lambda\left(1-\lambda^2\right)}{\lambda-\left(1-\lambda^2\right)\ln\sqrt{(1+\lambda)/(1-\lambda)}} \qquad (4.12a)$$

$$\sigma_{\perp} = \left(\frac{2}{3}\right)\frac{\lambda\left(1-\lambda^2\right)}{\left(1+\lambda^2\right)\ln\sqrt{(1+\lambda)/(1-\lambda)}-\lambda} \qquad (4.12b)$$

and

$$\lambda = \frac{\sqrt{r_{//}^2 - r_{\perp}^2}}{r_{//}} \ , \qquad 0 < \lambda \leqq 1. \qquad (4.13)$$

The symbols of k_B, η and T are Boltzman constant, viscosity of solvent and temperature, respectively.[16] The $r_{//}$ and $r_{\perp}$ values were calculated to be 3.9 and 2.6 Å, respectively by a DFT calculation method for PADS as described in Chapter 2, which gives $\sigma_{//}$ = 0.41 and $\sigma_{\perp}$ = 0.55 by use of equations (4.12a) and (4.12b), respectively. From these values and equation (4.10), the $\tau_{//}$ and $\tau_{\perp}$ values are finally calculated as theoretical values on the basis of the hydrodynamic diffusion theory.

First, the rotational anisotropy is examined. Theoretical rotational anisotropy value, N, can be calculated by the $\tau_{//}$ and $\tau_{\perp}$ values. According to equations (4.8) and (4.10)-(4.13), the N value follows the equation

$$N = \frac{\tau_{\perp}}{\tau_{//}} = \frac{\sigma_{//}}{\sigma_{\perp}} \qquad (4.14)$$

As seen in equations (4.12a) and (4.12b), the $\sigma_{//}$ and $\sigma_{\perp}$ values are determined only by the geometric structure of solute ($\sigma_{//}$ and $\sigma_{\perp}$) and the resultant N value is calculated to be 1.4 for PADS solute. This theoretical N value number is closer to the experimental N

value of 2.4 in organic solvent, *N*-methylimidazole, than ca. 3~5 in RTILs. The larger *N* value means the rotation of PADS around the perpendicular axis takes place more slowly than that around the parallel y-axis. The PADS radical has two sulfonyl groups with negative charges, and Coulombic interaction between the sulfonyl groups and cations of RTILs may hinder the rotation of PADS around the perpendicular axis. This might be a reason why the anisotropy of PADS (3~5) in RTILs is much larger than the *N* value (1.4) estimated by theory. Coulombic interaction between solute and solvent will expected to be less effective in organic solvent (*N*-methylimidazole) than in RTILs.

Secondly, the absolute value of rotation correlation times, $\tau_{\perp}$ and $\tau_{//}$ is discussed. For this purpose, we examine the temperature dependence of rotation correlation times by comparing the experimental values with the theoretical estimation is examined. Theoretical $\tau_{\perp}$ and $\tau_{//}$ values for a prolate top molecule in the liquid can be calculated according to equations (4.10) to (4.13) and their temperature dependence is plotted by solid lines in Figure 4.5. By comparing the theoretical lines with the experimental $\tau_{\perp}$ and $\tau_{//}$ values, it was found that theoretical values are longer than experimental values in all solvents in all the temperature range. This means microscopic viscosity around the solute is lower than macroscopic viscosity of solvent. Hence, the boundary conditions between solute and solvent on rotational motion are described below.

According to Youngren and Acrivos,[17] equation (4.10) is modified as

$$\tau_{\mathrm{i}}^{\mathrm{j}} = \frac{1}{6D_{\mathrm{i}}} C_{\mathrm{i}}^{\mathrm{j}} \quad (\mathrm{i} = // \; or \; \perp) \qquad (4.15)$$

The C_i^j coefficient with j = "stick" or "slip" is a parameter to specify the boundary condition between solute and solvent. If the boundary condition is "stick", the solute sticks to surrounding solvent molecules and no angular momentum transfer occurs between solute and solvent during rotation. The above-mentioned hydrodynamic diffusion theory for equations (4.9)-(4.13) assumes a stick boundary condition or C_i^{stick} =1. If the boundary condition is "slip", the solute rotates with slipping on surrounding solvent molecules. Under the slip boundary condition, a solute molecule of prolate top rotates around the parallel axis without any friction, which implies $C_{//}^{slip}$=0. When the solute rotates around the perpendicular axis, the prolate top rotor must encounter with surrounding solvent molecules, which implies $C_{\perp}^{slip}$ >0.

According to the literatures of Youngren and Acrivos[17] and of Sension and Hochstrasser[18], the $C_{\perp}^{slip}$ value is determined by the $r_{//}$ / $r_{\perp}$ ratio and calculated to be ~0.09 in the particular case of PADS. This value for the $C_{\perp}^{slip}$ value of PADS was adopted. The $\tau_{\perp}$ values in (a) $BmimTf_2N$, (b) *N*-methylimizaole, and (c) $BmimBF_4$ solutions were calculated for slip boundary conditions and the resultant curves are plotted by dotted lines in Figure 4.5. The measured $\tau_{\perp}$ times are shorter than the calculated $\tau_{\perp}^{stick}$ times (solid lines) but longer than the calculated $\tau_{\perp}^{slip}$ times (dotted lines). This observation means that the microscopic viscosity around the solute rotor is much smaller than the macroscopic viscosity of solvent but can not be neglected judging from a fact that $\tau_{\perp} > \tau_{\perp}^{slip}$. Thus, it was found that our measured $\tau_{\perp}$ values are reasonably explained by a Youngren and Acrivos's theory. For the rotation around

parallel y-axis, the experimental $\tau_{//}$ values are much shorter than the theoretical $\tau_{\perp}^{stick}$ values. The theoretical $C_{//}^{slip}$ value equals to zero and thus, the quantitative discussion on the measured $\tau_{//}$ value based on the hydrodynamic theory must be stopped. Another hydrodynamic theory will be examined instead in the subsequent section.

(4.3.4) Theoretical evaluation due to non-spherical slip model for isotropic rotation of PADS radical

According to Perrin,[19] the rotational correlation times of non-spherical solute can be described by introducing an *f*-parameter for SED equation of spherical solute. This parameter is dimensionless hydrodynamic frictional coefficient and depends on the shape of solute. Hu and Zwanzig[20] modified the equation by considering the boundary conditions and the shape of solute, which is represented by a coefficient, C_i. These modifications give equation (4.16).

$$\tau_R^i = \frac{V_p \eta}{k_B T} f C_i , \quad (\text{i = stick or slip}) \qquad (4.16)$$

Here, C_{stick} =1 and C_{slip} = 0.075 for the shape of PADS.[20] For the solute of prolate top shape, the *f*-parameter is expressed by

$$f = \frac{2}{3R} \frac{\left(R^2+1\right)\left(R^2-1\right)^{3/2}}{\left(2R^2-1\right)\ln\left(R+\sqrt{R^2-1}\right) - R\sqrt{R^2-1}} \qquad (4.17)$$

where R means $r_{\perp}/r_{//}$.[19,21] The f-value of PADS is 1.18, and V_p is a volume of solute.

Since the theory provides mean value of τ_R, we employed τ_R^{obs} which is obtained by

averaging experimental values of $\tau_{//}$ and $\tau_{\perp}$ according to the following equation.

$$\tau_R^{obs} = \sqrt{\tau_{//}\tau_{\perp}} \qquad (4.18)$$

This treatment is after the method done by Freed and coworkers.[4] To compare the measured τ_R^{obs} values with calculated τ_R^{stick} and τ_R^{slip} values, the observed and calculated τ_R values of PADS were plotted against η/T in (a) $BmimTf_2N$, (b) *N*-methylimidzole, (c) $DemeTf_2N$ and (d) $N_{3111}Tf_2N$ as shown in Figure 4.6. The similar plots for PADS dissolved in solvents of (a) $BmimBF_4$ and (b) $BmimPF_6$ are shown in Figure 4.7. One can recognize from Figure 4.6 that the τ_R^{obs} values are located between two theoretical lines corresponding to τ_R^{stick} and τ_R^{slip} estimations. This indicates that τ_R^{obs} in $BmimTf_2N$, *N*-methylimidzole, $DemeTf_2N$ and $N_{3111}Tf_2N$ can be explained by the hydrodynamic theory modified with lowering of the microscopic viscosity.[20] On the other hand, Figure 4.7 shows that the τ_R^{obs} times measured in $BmimBF_4$ and $BmimPF_6$ solvents are even shorter than the τ_R^{slip} values. The experimental results shown in Figure 4.7 can not be interpreted by Hu and Zwanzig theory with slip boundary condition and may be categorized as so-called "subslip" boundary condition. The calculated $\tau_R^{obs}/\tau_R^{slip}$ ratios are listed in Table 4.4. Most of the ratios are larger than unity, and possively the rotation of PADS in those solvents can be characterized by Hu and Zwanzig theory. On the other hand, the $\tau_R^{obs}/\tau_R^{slip}$ ratios derived for the $BmimBF_4$ and $BmimPF_6$ solutions are smaller than unity, and Hu and Zwanzig theory can not explain the experimental results or the boundary condition seems to fall into a "subslip" region. Some modification is needed to equation (4.16) derived by Hu and Zwanzig theory.

Fruchey *et al*.[1] have recently reported on similar subslip rotation of dye molecule in alkyl-substituted imidazolium-based RTILs. The "subslip" boundary condition usually originates from the inhomogeneous nature of solvent, which can not be characterized by one macroscopic viscosity value. They have proposed that fast rotation in RTIL may be due to selective solvation of dye molecule in a hypothetical non-polar and low-viscous region of RTIL. This interpretation may not be applicable for PADS because PADS has two sulfonyl groups with negative charges and may dissolve in a polar region of RTIL.

Recently, Yao and coworkers reported the frequency dependence of shear viscosity η for PF_6-based RTILs with 1-alkyl-3-methylimidazolium cations in their sound absorption and velocity measurements.[22] More recently, Yamaguchi and Koda[23] measured the frequency-dependent η values of $BmimPF_6$ and $BmimTf_2N$ at 298 K for a frequency range of 0 to 0.2 GHz. It is striking that the η values of $BmimTf_2N$ are almost constant in this frequency range, whereas the values of $BmimPF_6$ are prominently dependent on the frequency. For example, the shear viscosity at 0.2 GHz becomes about one third of the zero-frequency value. They roughly estimated Debye relaxation time of 1.1 ns at 298K in $BmimPF_6$. This relaxation time is close to the present τ_R^{obs} value of 0.6ns for PADS in $BmimPF_6$. These experimental observations suggest that the subslip rotation in $BmimPF_6$ found in this study may originate from lowering of shear viscosity for the PADS rotational diffusion at high frequency. Unfortunately, no experimental data on the frequency dependent η is available for $BmimBF_4$, but similar "subslip" nature

due to lowing of macroscopic shear viscosity at high rotational frequencies would also be expected in $BmimBF_4$ as well as in $BmimPF_6$.

(4.3.5) Fractional η/T dependence of rotational correlation time in $BmimPF_6$

Finally, another experimental finding recognized in Figure 4.7 is discussed. It is interesting to note that the slopes in Figure 4.7, log (τ_R^{obs})/ log (η/T), are not unity, though they are nearly unity in Figure 4.6 and in the similar plots for most of RTILs used here. It is assumed that the experimental data points follow the equation,

$$\tau_R^{obs} \propto \left(\frac{\eta}{T}\right)^t \qquad (4.19)$$

where a fractional parameter of t is introduced to correct η/T dependence as explained in Chapter 3. The t values determined are listed in Table 4.4. If rotational motion follows hydrodynamic theory with equation (4.16), the t values are unity. It is noteworthy that t values are actually unity in RTILs having relatively large anions of Tf_2N or $C_2H_5OSO_3$. On the other hand, t values are clearly less than unity in the solvents of $BmimBF_4$, $BmimPF_6$ and $DemeBF_4$. This means the dependence of τ_R^{obs} on η/T is different from the hydrodynamic estimation in the latter three solvents. In Chapter 3, the similar $t < 1$ relation for rotation of proxyl radicals in $BmimPF_6$ and in $BmimBF_4$ was indicated. As discussed in the above section for subslip nature of rotation in $BmimPF_6$ and $BmimBF_4$, it was assumed that the shear viscosity, $\eta_{R,}$ of these solvents at the high frequencies of PADS rotation deviates from the shear viscosity of η at zero-frequency, which roughly

follows Debye relaxation function. Then, it was expected that the η_R/η ratio around Debye relaxation frequency will decrease as temperature increases. This description accords with the experimental relation that $t < 1$ for these three RTILs. In contrast to the result in $BmimPF_6$, η_R is close to η at zero-frequency for $BmimTf_2N$[23] at 298K and the η_R/η ratio is thus expected to be around unity for $BmimTf_2N$ at higher temperatures employed in the present study. This gives parameter t of unity as shown in the present experiment. There are several literatures reporting parameter t of unity for rotation of large and fluorescent dye molecules in $BmimPF_6$.[3,24,25] The τ_R^{obs} values of these molecules at 298K are around 10ns which is much longer than relaxation time for shear viscosity. This may be why the τ_R^{obs} values for these dye molecules follow hydrodynamic equation with $t = 1$. On the contrary, Wakai *et al*. reported $t = 0.63$ and 0.82 for D_2O and C_6D_6 in $BmimPF_6$ with τ_R^{obs} values of 0.2ns and 0.7ns, respectively, by means of NMR measurements.[26] Their results showing the sub-nanosecond τ_R^{obs} value with a relation that $t < 1$ rather accord with ours in $BmimPF_6$. Similarly, proxyl radicals show the τ_R^{obs} value of about 2ns giving the $t = 0.7$ relation in $BmimPF_6$ and $BmimBF_4$ in Chapter 3. These small solutes of PADS, proxyl radicals, D_2O and C_6D_6 exhibit relatively fast rotation and thus, rotation dynamics presumably relates to relaxation of shear viscosity. Although evaluation of this mechanism requires further detailed analysis on τ_R^{obs} values, the frequency dependent shear viscosity is considered to be quite important for understanding solute rotation in RTILs.

(4.4) Conclusion

This chapter focuses on the rotation motion and solvation of PADS nitroxide radical dissolved in various RTILs. By analyzing the EPR spectra, the hyperfine coupling constant (A), the temperature-dependent anisotropic rotational correlation times ($\tau_{//}$ and $\tau_{\perp}$), and the rotational anisotropy(N) defined as $\tau_{\perp}/\tau_{//}$ were determined. The A values are constant for almost all RTILs (Table 4.1), which indicates negligible interaction between the N-O group and the cation of RTILs. Secondly, the N values determined in RTILs and N-methylimidazole solvents are compared with the N value of 1.4 calculated by hydrodynamic theory (Table 4.2). The N value of 2.4 for N-methylimidazole solvent is slightly larger than 1.4 but still close to the value calculated by hydrodynamic theory. On the other hand, the N values determined in RTIL solvents are 3 ~ 5 and apparently larger than 1.4. The interaction between the sulfonyl groups of PADS and the cation of RTILs seems to prolong the $\tau_{\perp}$ lifetimes in RTILs, which leads to larger N values in RTILs. Thirdly, experimental values of $\tau_{//}$ and $\tau_{\perp}$ are compared with those calculated by hydrodynamic theory. Almost all the experimental values are shorter than the calculated τ_R^{stick} values but longer than the calculate τ_R^{slip} values (Figure 4.6). The hydrodynamic theory with the slip boundary condition seems to give better agreement with the experimental τ_R^{obs} values. In some RTILs, experimental τ_R values are still shorter than the calculated τ_R^{slip} values. Finally, the η/T dependence of rotational correlation times is evaluated by equation (4.19) using a parameter of t. The t values are normally close to unity but the values below unity are derived from the experiments obtained in

$BmimBF_4$, $BmimPF_6$ and $DemeBF_4$ solvents (Table 4.4). On the basis of Debye relaxation of shear viscosity in $BmimPF_6$ reported recently, one plausible mechanism responsible for the $t < 1$ relation observed in these RTILs was discussed.

(a)

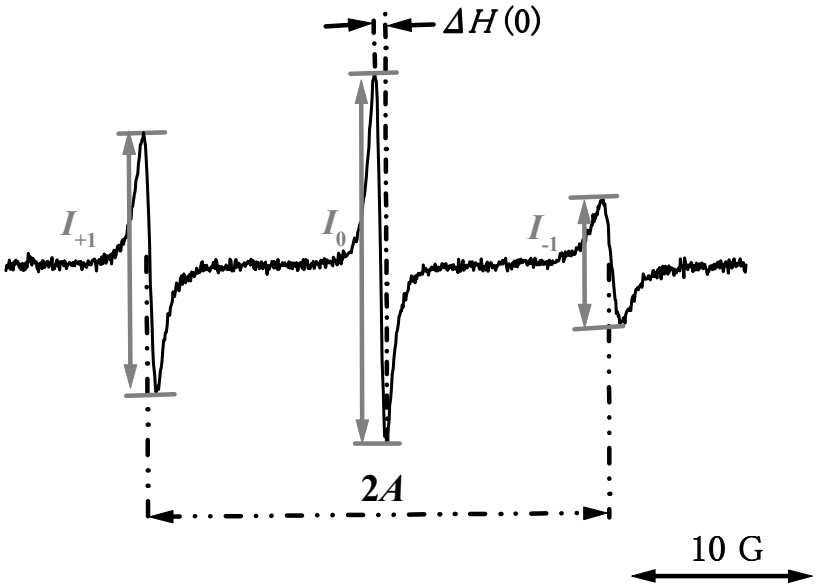

(b)

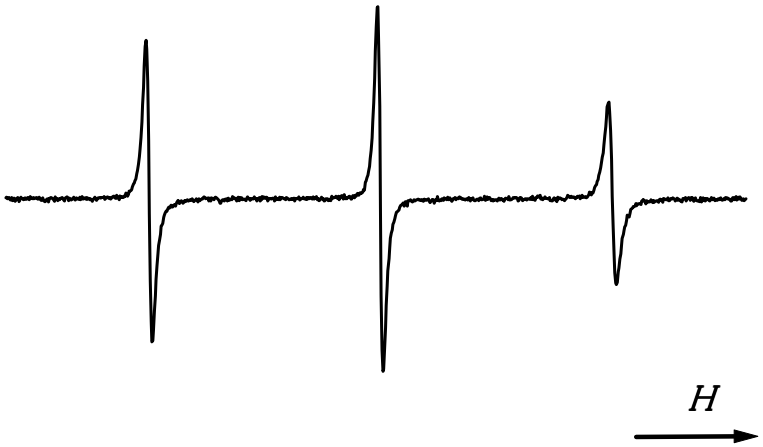

Figure 4.1: EPR spectra of PADS in $BmimPF_6$ measured at (a) 295 K and (b) 320 K. The parameters used for equations (2) and (3) are given in (a).

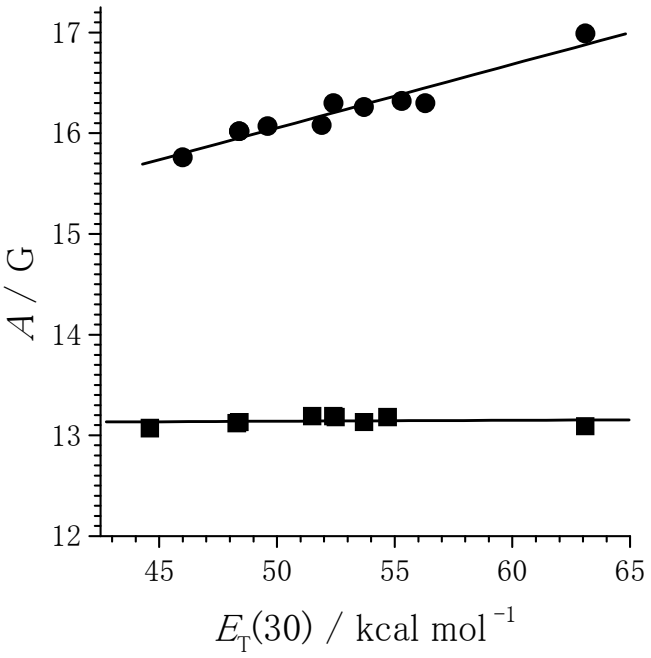

Figure 4.2: Plots of A vs. $E_T(30)$ values for ATEMPO (●) and PADS (■) radicals dissolved in various RTILs and conventional solvents.

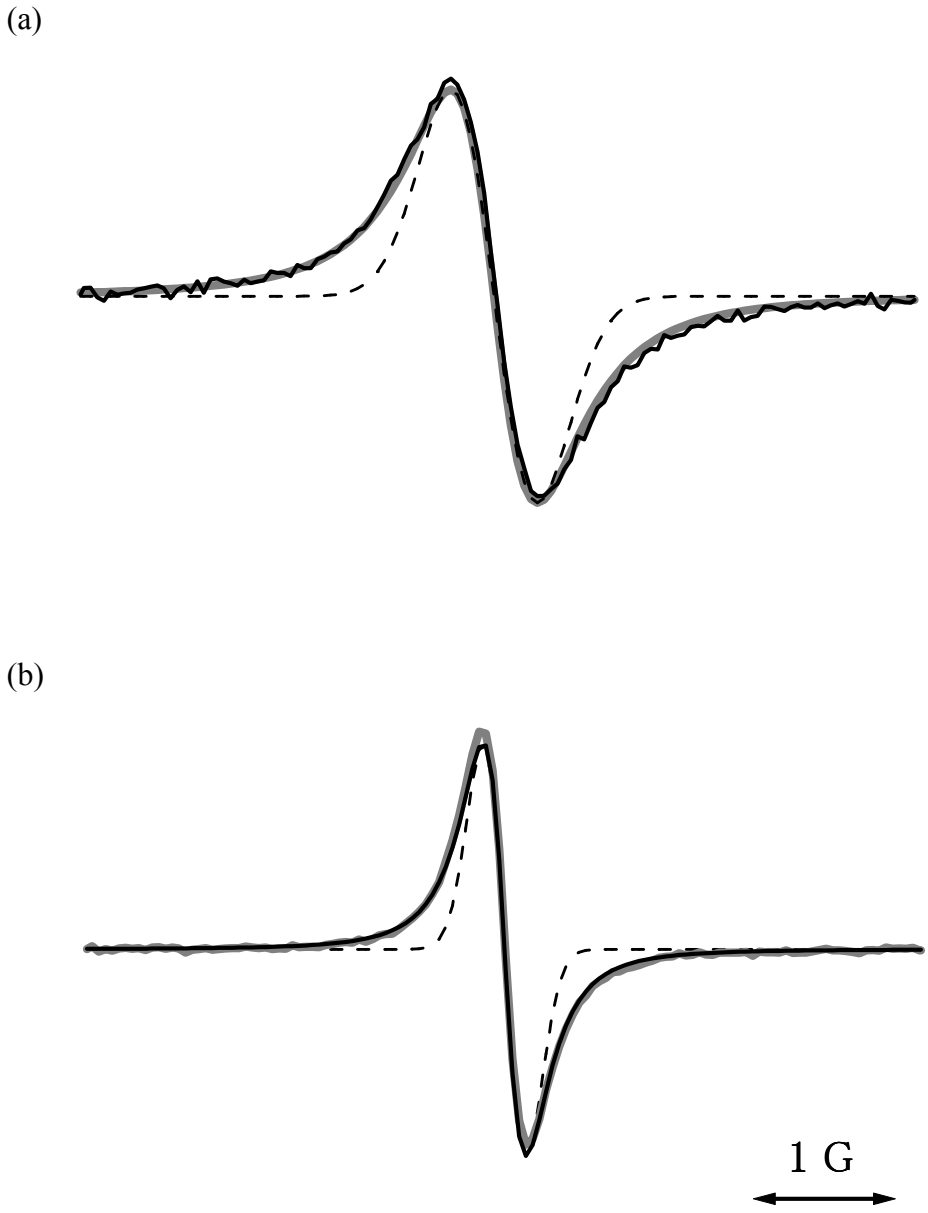

Figure 4.3: EPR spectra of PADS radicals dissolved in $BmimPF_6$ recorded at (a) 295 K and (b) 320 K. The spectra are simulated by Lorentzian (gray lines) and Gaussian (dashed lines) lineshapes.

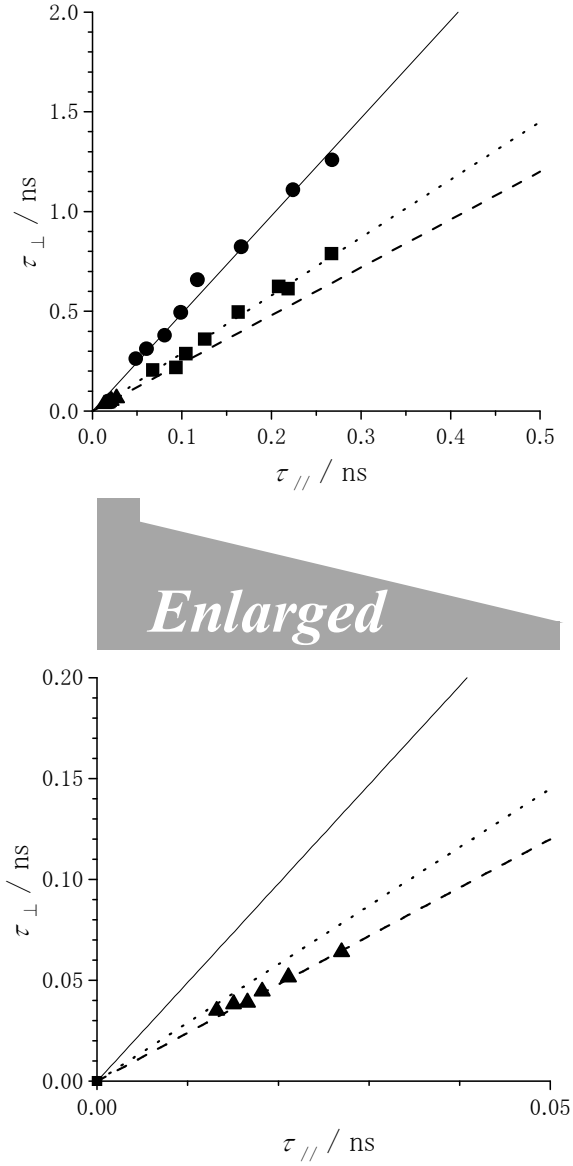

Figure 4.4: Relation plots of $\tau_{\perp}$ vs. $\tau_{//}$ values of PADS radical measured in three solvents. The solvents were $BmimCH_3OSO_3$ (■), $DemeTf_2N$ (●) and *N*-methylimidazole (▲). Solid, dotted and dashed lines were obtained by least-squares fittings with *N* values of 4.9, 2.9 and 2.4, respectively.

(a) $BmimTf_2N$

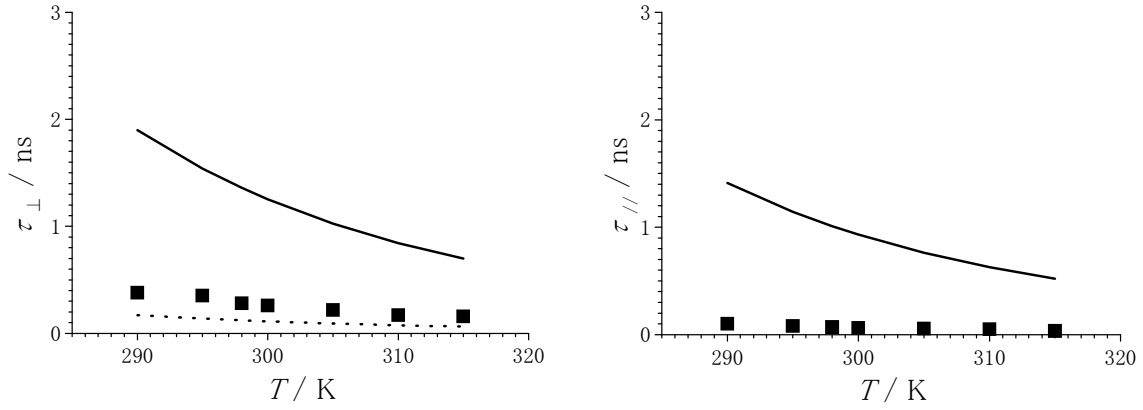

(b) *N*-methylimidazole

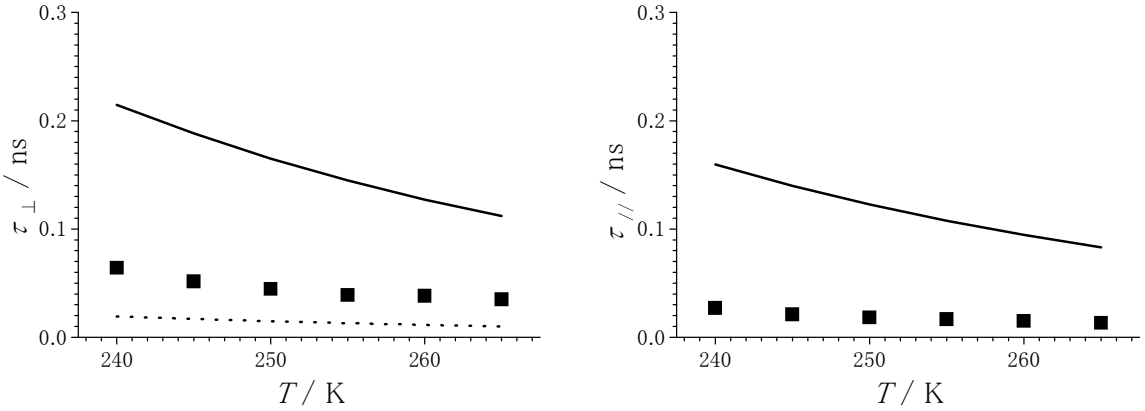

(c) $BmimBF_4$

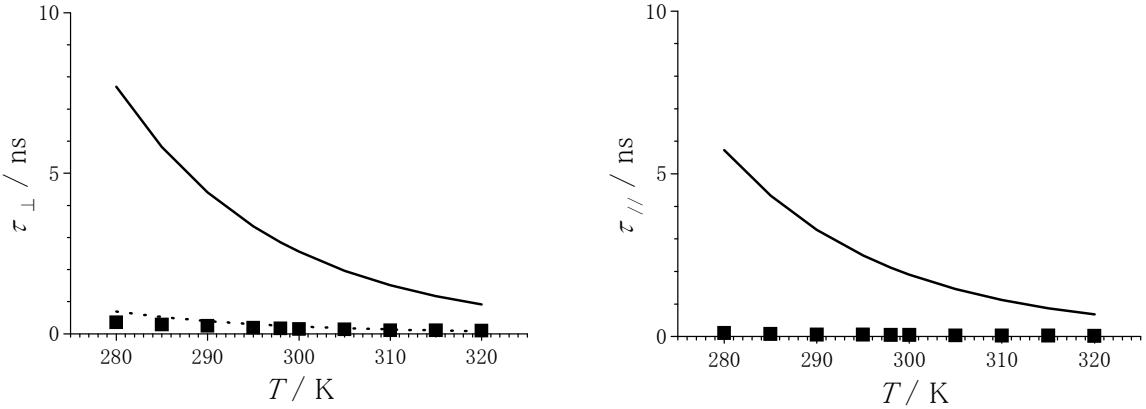

Figure 4.5: Plots of rotational correlation times of $\tau_{\perp}$ and $\tau_{//}$ vs. T measured in three solvents: (a) $BmimTf_2N$, (b) *N*-methylimidazole and (c) $BmimBF_4$. The experimental data are presented by filled squares (■). The simulations based on hydrodynamic diffusion theory are shown by solid and dotted lines, which are calculated under stick and slip boundary conditions, respectively.

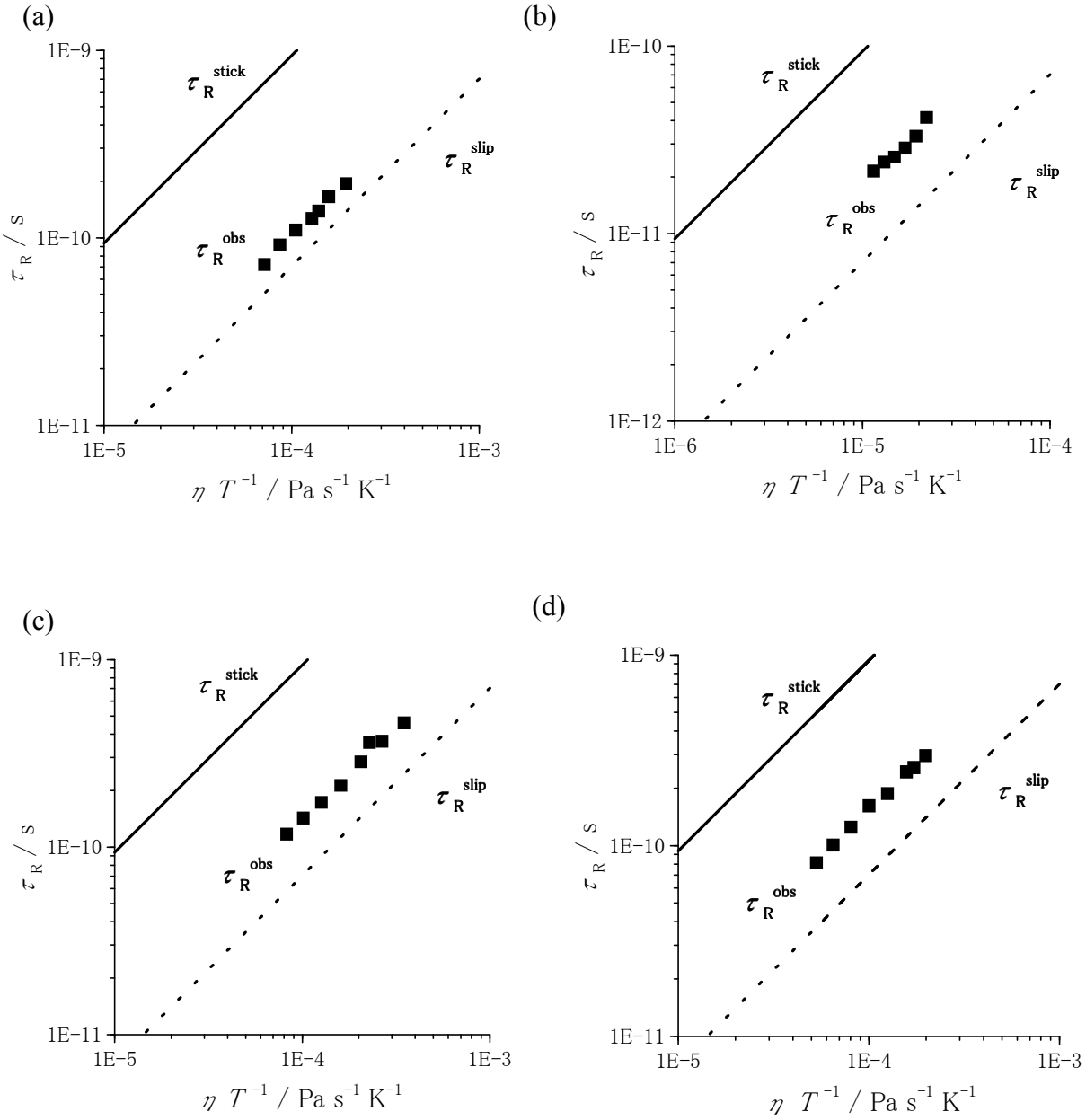

Figure 4.6: Logarithmic plots of measured τ_R values (■) of PADS vs. $\eta\ T^{-1}$ in (a) $BmimTf_2N$, (b) *N*-methylimidazole, (c) $DemeTf_2N$ and (d) $N_{3111}Tf_2N$. Theoretical τ_R values calculated under the stick and slip conditions are shown by solid and dotted lines, respectively (see text for the details).

(a)

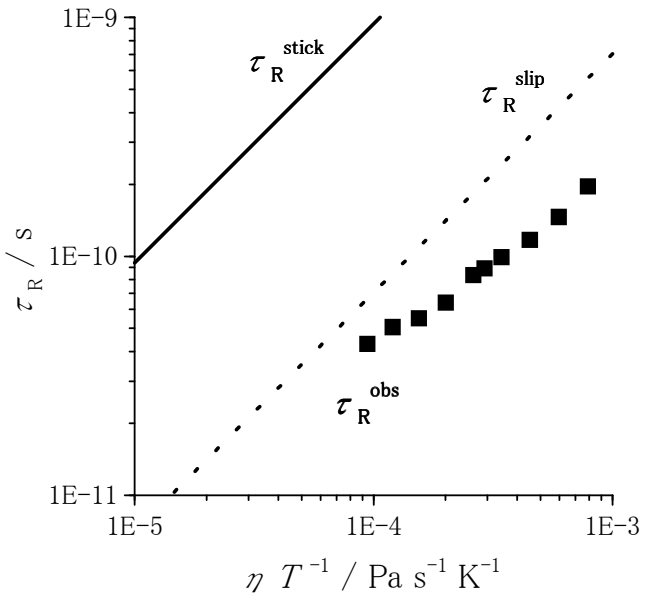

(b)

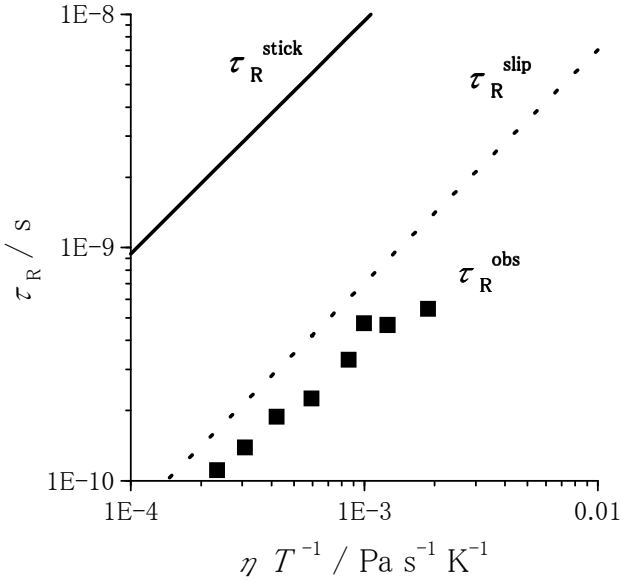

Figure 4.7: Logarithmic plots of measured τ_R values (■) of PADS vs. $\eta\ T^{-1}$ in (a) $BmimBF_4$ and (b) $BmimPF_6$. Theoretical τ_R^{stick} and τ_R^{slip} values are shown by solid and dotted lines, respectively.

Table 4.1: A summary of *g* and *A* values of PADS in various solvents

solvents	*g* value	*A* value / G	$E_T(30)$ / kcal mol^{-1}
$Py_{14}Tf_2N$	2.0054	13.12	48.2 [a]
$N_{3111}Tf_2N$	2.0055	13.06	
$BmimTf_2N$	2.0055	13.19	51.5 [b]
$EmimBF_4$	2.0055	13.13	53.7 [c]
$BmimBF_4$	2.0054	13.18	52.2 – 53.9 [a,d]
$DemeTf_2N$	2.0057	13.13	48.4 [d]
$EmimC_2H_5OSO_3$	2.0054	13.16	
$BmimPF_6$	2.0054	13.19	52.3-53.9 [b,d,e]
$DemeBF_4$	2.0056	13.13	48.4[d]
$BmimCH_3OSO_3$	2.0056	13.21	
$PP_{13}Tf_2N$	2.0054	13.09	
$Py_{13}Tf_2N$	2.0054	13.11	
N-methylimidazole	2.0053	13.07	44.6[e]
H_2O	2.0055[f]	13.09[f]	63.1[g]

[a]From ref 13. [b]From ref 11. [c]From ref 12. [d]From ref 8. [e]From ref 10. [f]From ref 4. [g]From ref 7.

Table 4.2: Rotational anisotropy of PADS.

	Solvent	rotational anisotropy (N)
Experiment	RTILs	
	$BmimCH_3OSO_3$	4.9 ± 0.1 [a]
	$BmimPF_6$	4.6 ± 0.1 [a]
	$DemeBF_4$	4.3 ± 0.1 [a]
	$EmimC_2H_5OSO_3$	4.1 ± 0.1 [a]
	$PP_{13}Tf_2N$	4.0 ± 0.2 [a]
	$BmimTf_2N$	4.0 ± 0.1 [a]
	$EmimBF_4$	4.0 ± 0.1 [a]
	$BmimBF_4$	3.6 ± 0.1 [a]
	$Py_{14}Tf_2N$	3.5 ± 0.1 [a]
	$N_{3111}Tf_2N$	3.2 ± 0.2 [a]
	$Py_{13}Tf_2N$	3.2 ± 0.1 [a]
	$DemeTf_2N$	2.9 ± 0.1 [a]
	Organic solvent	
	N-methylimidazole	2.4 ± 0.1 [a]
Calculation	------	1.4 [b]

[a]Determined by equation (4.14) using experimental data ($\tau_{\perp}$ and $\tau_{//}$) for various solvents.

[b]Calculated by equations (4.10-14) and the values of $r_{//}$ (3.9 Å) and $r_{\perp}$(2.6 Å).

Table 4.3: Activation energy for the rotational motion of PADS.

	perpendicular rotation [a]	parallel rotation [b]
solvents	E_a (⊥) / kJ・mol^{-1}	E_a (//) / kJ・mol^{-1}
$EmimBF_4$	23.7 ± 1.1	31.0 ± 2.0
$BmimBF_4$	25.0 ± 1.0	30.8 ± 1.3
$BmimTf_2N$	29.9 ± 2.9	28.7 ± 1.9
$Py_{13}Tf_2N$	32.4 ± 1.5	32.3 ± 1.6
$EmimC_2H_5OSO_3$	34.0 ± 1.0	40.2 ± 1.1
$N_{3111}Tf_2N$	35.2 ± 1.7	33.3 ± 1.4
$Py_{14}Tf_2N$	37.7 ± 3.1	37.7 ± 1.8
$DemeTf_2N$	38.0 ± 2.0	35.5 ± 1.6
$BmimCH_3OSO_3$	40.7 ± 0.6	42.4 ± 0.9
$PP_{13}Tf_2N$	43.5 ± 1.8	32.7 ± 2.3
$BmimPF_6$	46.1 ± 2.1	42.8 ± 3.2
$DemeBF_4$	50.1 ± 1.4	44.1 ± 0.8
N-methylimidazole	12.3 ± 1.1	14.2 ± 1.1

[a]Rotational motion around an axis on the xz plane perpendicular to the y-axis (Chart 1).

[b]Rotational motion around the y-axis.

Table 4.4: Comparison of experimental and theoretical τ_R as a function of temperature or viscosity.

solvent	*t*-parameter [a]	τ_R^{obs} / τ_R^{slip} [b]
$BmimBF_4$	0.70 ± 0.02	0.35 ~ 0.65 [c]
$BmimPF_6$	0.82 ± 0.05	0.41 ~ 0.67 [c]
$DemeBF_4$	0.84 ± 0.02	1.57 ~ 1.97 [c]
$PP_{13}Tf_2N$	0.90 ± 0.03	1.12
$BmimCH_3OSO_3$	0.91 ± 0.01	1.53
$Py_{13}Tf_2N$	0.94 ± 0.03	1.16
$Py_{14}Tf_2N$	0.96 ± 0.05	1.63
$BmimTf_2N$	0.96 ± 0.04	1.45
$N_{3111}Tf_2N$	0.97 ± 0.02	2.17
$DemeTf_2N$	0.99 ± 0.03	1.98
$EmimC_2H_5OSO_3$	1.06 ± 0.03	1.35
$EmimBF_4$	1.09 ± 0.05	1.19
N-methylimidazole	0.96 ± 0.07	2.53

[a]Parameters were determined by fitting the data to equation (4.19). [b]The τ_R^{obs} values are derived by equation (4.18) and experimental data on $\tau_{//}$ and $\tau_{\perp}$. The τ_R^{slip} values are estimated by equation (4.16) under the slip condition (C_{slip}=0.075). [c]The values depend on the temperature.

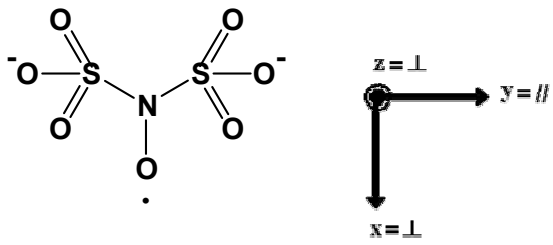

Chart 4.1: Structure of PADS and molecular axes employed.

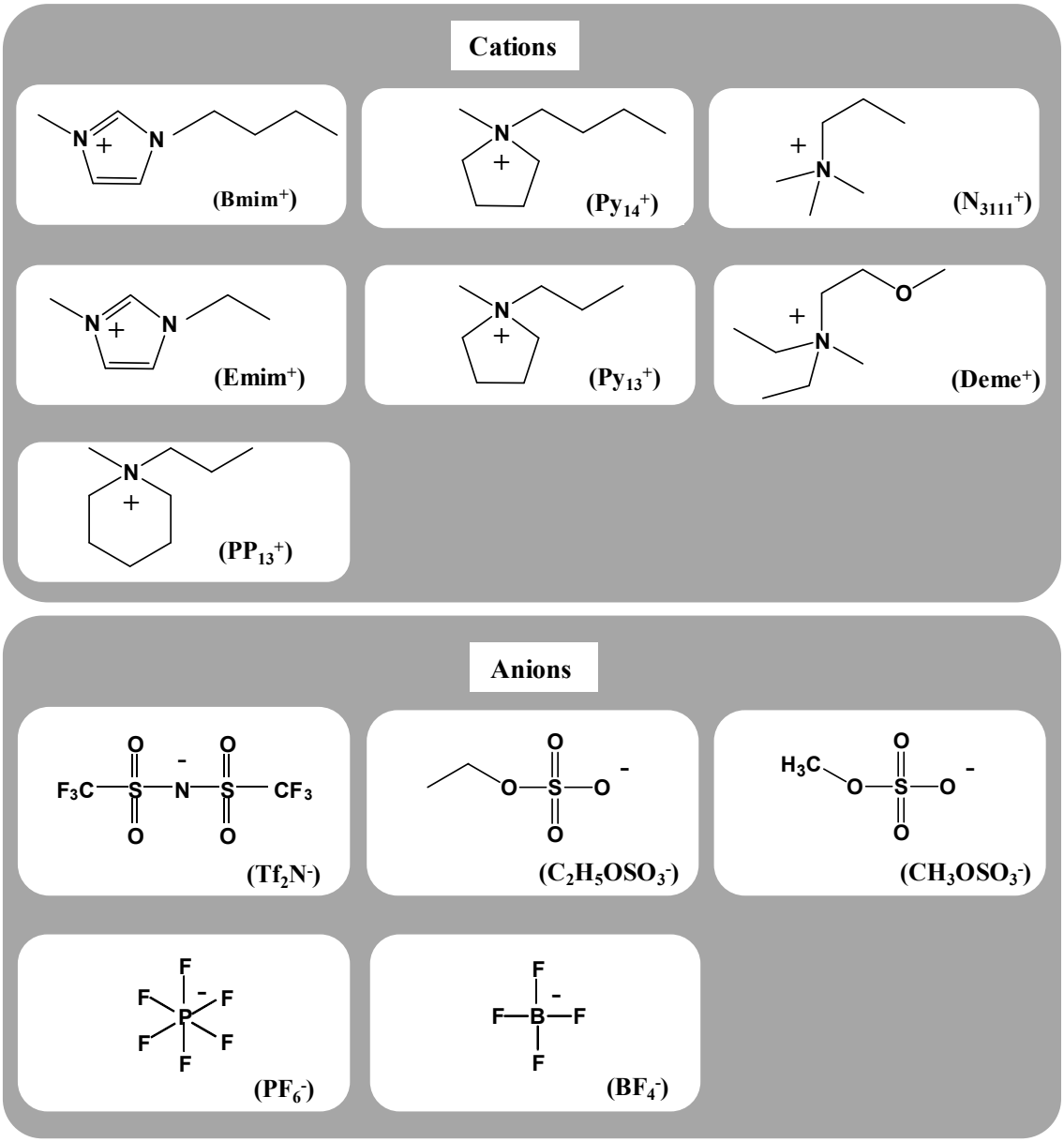

Chart 4.2: Structures of cations and anions in RTILs and their abbreviates.

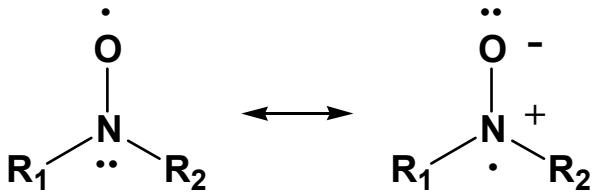

Chart 4.3: Two canonical structures of nitroxide.

References and a note of Chapter 4

(1) Fruchey, K.; Fayer, M. D. *J. Phys. Chem. B* **2010**, *114*, 2840.

(2) Ito, N.; Arzhantsev, S.; Maroncelli, M. *Chem. Phys. Lett*. **2004**, *396*, 83.

(3) Jin, H.; Baker, G.; Arzhantsev, S.; Dong, J.; Maroncelli, M. *J. Phys. Chem. B* **2007**, *111*, 7291.

(4) Goldman, S. A.; Bruno, G. V.; Polnaszek, C. F.; Freed, J. H. *J. Chem. Phys*. **1972**, *56*, 716.

(5) Emim; 1-ethyl-3-methylimidazolium, N_{3111}; *N*, *N*, *N*-trimethyl-*N*-propylammonium, Py_{14}; *N*-methyl-*N*-propylpyrrolidinium, Py_{13}; *N*-methyl-*N*-propylpyrrolidinium, PP_{13}; *N*-methyl-*N*-propylpiperidinium, Deme; *N*, *N*,-diethyl-*N*-methyl-*N*-(2-methoxyethyl)ammonium

(6) Drago, R. S. *J. Chem. Soc., Perkin Trans. 2* **1992**, 1827.

(7) Knauer, B. R.; Napier, J. J. *J. Am. Chem. Soc.* **1976**, *98*, 4395.

(8) Kawai, A.; Hidamori, T.; Shibuya, K. *Chem. Lett.* **2004**, *33*, 1464.

(9) Reichardt, C. *Chem. Rev.* **1994**, *94*, 2319.

(10) Mellein, B. R.; Aki, S. N. V. K.; Ladewski, R. L.; Brennecke, J. F. *J. Phys. Chem. B* **2007**, *111*, **131**.

(11) Muldoon, M. J.; Gordon, C. M.; Dunkin, I. R. *J. Chem. Soc. Perkin Trans. 2* **2001**, *4*, 433.

(12) Park, S.; Kazlauskas, R. J. *J. Org. Chem*. **2001**, *66*, 8395.

(13) Tokuda, H.; Tsuzuki, S.; Susan, M. A. B. H.; Hayamizu, K.; Watanabe, M. *J.*

Phys. Chem. B **2006**, *110*, 19593.

(14) Robinson, R.; Thomann, H.; Beth, A.; Fajer, P.; Dalton, L. *EPR and Advanced EPR Studies of Biological Systems*; CRC, Boca Raton, 1985; Chap. 2.

(15) Atherton, N. M. *Principles of Electron Spin Resonance*; Ellis Harwood, Chichester, 1993; Chap.9.

(16) Hwang, J. S.; Mason, R. P.; Hwang, L. P.; Freed, J. H. *J. Phys. Chem.* **1975**, *79*, 489.

(17) Youngren, G. K.; Acrivos, A. *J. Chem. Phys*. **1975**, *63*, 3846.

(18) Sension, R. J.; Hochstrasser, R. M. *J. Chem. Phys.* **1993**, *98*, 2490.

(19) Perrin, F. J. *J. Phys. Radium*, **1936**, *7*, 1.

(20) Hu, C. M.; Zwanzig, R. *J. Chem. Phys*. **1974**, *60*, 4354.

(21) Roy, M.; Doraiswamy, S. *J. Chem. Phys*. **1993**, *98*, 3213.

(22) Makino, M.; Kishikawa, R.; Mizoshiri, M.; Takeda, S.; Yao, M. *J. Chem. Phys.* **2008**, *129*, 104510.

(23) Yamaguchi, T.; Miyake, S.; Koda, S. *J. Phys. Chem. B* **2010**, *114*, 8126.

(24) Khara, D. C.; Samanta, A. *Phys. Chem. Chem. Phys*. **2010**, *12*, 7671.

(25) Mali, K. S.; Dutt, G. B.; Mukherjee, T. *J. Chem. Phys*. **2005**, *123*, 174504.

(26) Yasaka, Y.; Wakai, C.; Matsubayashi, N.; Nakahara, M. *J. Chem. Phys*. **2007**, *127*, 104506.

Chapter 5. Solute size and shape dependent rotational diffusion in RTILs

(5.1) Introduction

In Chapter 4, rotational correlation times, τ_R^{obs}, of PADS nitroxide radical dissolved in various RTILs were measured by EPR spectroscopy. Important experimental findings are the summarized as the following two points: (1) the τ_R^{obs} values are longer than those calculated by hydrodynamic theory with slip boundary condition, namely τ_R^{slip}, and, (2) the τ_R^{obs} values are exceptionally shorter than τ_R^{slip} values in $BmimPF_6$ and in $BmimBF_4$ which are composed of relatively small anions. These results indicate that rotation motion of PADS solutes depends on ion components of RTILs. Contrary to the EPR experiments described in Chapter 4 where chemical characters of RTILs were examined for PADS rotation, this chapter focused on the effect of solute character on rotation motion.

It is worthwhile to address that solute size effect on rotational diffusion has been examined widely in molecular solvents.[1-3] Ben-Amotz *et al.* reported the solute size effect on rotational diffusion. They indicated that rotational correlation times of larger-sized solute gives nearly perfect agreement with hydrodynamic predictions with stick boundary condition in both alkane and alcohol solvents, while the experimental results showed an increasingly large deviation from the hydrodynamic predictions as the solute size decreased.[1] In this chapter, proxyl radicals which is larger in size than PADS,

was selected as solvent and the ratios of τ_R^{obs} to τ_R^{slip} measured in $BmimBF_4$, $BmimPF_6$ and $BmimTf_2N$ were determined to understand the solute size effect on hydrodynamic behavior of solute rotation in RTIL solvents. Another important investigation on solute rotation lies in solute shape dependence. In this chapter, nitroxide radicals, whose shapes are non-sphere or ellipse were employed as solute and the $\tau_R^{obs}/\tau_R^{slip}$ values were examined. The effect of solute size and shape on the rotation motion in RTILs is discussed by comparing the results of nitorxides including PADS in the previous chapter.

5.2 Experimental

Sample preparation, DFT calculation, measurements of EPR spectra, water content, and viscosity are described in Chapter 2. Samples used in this chapter were as follows. 3 β -DOXYL-5 α -chorestane, free radical (DOXYL) was purchased from Aldorich. 2,2,6,6-tetramethylpiperidine-1-oxyl (TEMPO) was purchased from Tokyo Kasei. The other samples are the same ones as described in Chapter 3 and Chapter 4. Structures of DOXYL and TEMPO as well as other nitroxide free radicals used in this chapter are summarized in Chart 5.1.

5.3 Results and Discussion

(5.3.1) Structure and size of nitroxide radicals

In the beginning, the size and shape of five nitroxide radicals, namely, PADS,

TEMPO, CProxylH, CProxyl$^-$ and DOXYL are discussed on the basis of quantum chemical calculation to clarify individual solute characters. The chemical structures of these radicals are shown in Chart 5.1. Volumes of these solute molecules were calculated by the DFT method as mentioned in Chapter 2. Molecular volumes of TEMPO, CProxylH and CProxyl$^-$ are 167, 204 and 219 Å^3, respectively. The literature value of 349 Å^3 was adopted for DOXYL,. It should be noted that these nitroxides are larger in volume than PADS, whose molecular volume is 110 Å^3 as already calculated in Chapter 4. These volume values are listed in Table 5.1.

The hydrodynamic radii, $r_{//}$ and $r_{\perp}$, are calculated for these nitorxide radicals to examine the shape of these molecules. The $r_{//}/r_{\perp}$ values of PADS, TEMPO, CProxylH and CProxyl$^-$ are in a range of 1.27 ~ 1.50, nearby unity. Therefore, the shape of TEMPO, CProxylH and CProxyl$^-$ are recognized as pseudo-sphere. On the other hand, the $r_{//}/r_{\perp}$ value of DOXYL is 3.4 and is classified into non-spheric and ellipse shape. The shape of PADS is approximated by prolate-top as explained in Chapter 4 but is close to sphere. In this view point, a group of PADS, TEMPO, CProxylH and CProxyl$^-$ belong to pseudo-sphere, while another group of PADS and DOXYL are approximated as prolate top molecules. In the former group, the radius of pseudo-sphere changes depending on the selection of solute. In the latter group, *f*-values of solute changes largely by a choice of solute whose ratio of hydrodynamic radii, $r_{//}$ and $r_{\perp}$ are remarkably different for PADS or DOXYL. The *f*-values of these nitroxides are calculated by the procedure introduced in Chapter 4, together with the $r_{//}$ and $r_{\perp}$ values.

These results were also listed in Table 5.1. According to this investigation on the shape and volume of five nitroxide radicals appearing in this chapter, the dependence of rotation dynamics on solutes character is argued as described below.

(5.3.2) EPR spectra measured for TEMPO and DOXYL nitroxide radicals dissolved in RTILs

Figure 5.1 (a) shows the EPR spectrum of TEMPO nitroxide radical in $BmimTf_2N$ at 270 K. The spectra show triplet hyperfine structure due to nuclear spin of ^{14}N as being similar to the spectra of PADS, CProxylH and $CProxyl^-$. To determine rotational correlation times on the basis of theory by Freed *et al*., the EPR spectral lineshape should be Lorentzian as noticed in Chapter 4. This requirement is satisfied in the EPR spectrum of TEMPO at 270 K in $BmimTf_2N$. This temperature is low, but is still above the melting point, 269K of $BmimTf_2N$.[4] Figure 5.1 (b) shows EPR spectrum of DOXYL nitroxide radical in $BmimPF_6$ at 350 K. The spectrum is also characterized by triplet peaks of Lorentzian lineshape. For simple analysis of EPR spectra to determine rotational correlation time, the radical rotation should be in "fast motion region". Unfortunately, DOXYL is so large that rotation correlation time is slower than other nitroxide in this study and the spectrum at 298 K is not in "fast motion region". Therefore, the temperature of solution was raised to 350 K to reduce viscosity so as to obtain the spectrum characterized by "fast motion region". At this temperature, the rotation of DOXYL in $BmPF_6$ became faster and the lineshape was found to be

Lorentzian. For the other samples, the experimental temperatures were appropriately controlled to satisfy the conditions in which the theory can be used.

(5.3.3) Volume dependent rotational correlation time of pseudo-sphere solutes in RTILs

First, the solute volume dependence on the rotational correlation time was examined in this section by using four pseudo-sphere nitroxide radicals with different volumes. Rotational correlation times, τ_R^{obs}, of TEMPO, CProxylH, CProxyl$^-$ and DOXYL were obtained by analyzing the EPR spectra and the resultant values are summarized in Table 5.1. The τ_R^{obs} values are compared with τ_R^{stick} and τ_R^{slip} values calculated by hydrodynamic theory with stick and slip boundary conditions according to Hu and Zwanzig theory as described in Chapter 4. For all the samples, the τ_R^{obs} values were found to be longer than the τ_R^{stick} values. This is essentially the same condition with those of PADS rotation in various RTILs. This means that the rotational diffusion of nitroxide radicals in RTILs cannot be explained by hydrodynamic theory with stick boundary condition.

To examine solute character dependence on rotational diffusion of solute in RTILs, the ratios of τ_R^{obs} to τ_R^{slip} were evaluated for PADS, TEMPO, CProxylH, CProxyl$^-$ in BmimPF$_6$, BmimBF$_4$ and BmimTf$_2$N. The results are summarized in Table 5.1. To examine the solute dependence of the rotation diffusion, the $\tau_R^{obs}/\tau_R^{slip}$ values are plotted against volumes of the solutes, V_p as shown in Figure 5.2. For PADS samples, $\tau_R^{obs}/\tau_R^{slip}$

values for $BmimBF_4$ and $BmimPF_6$ solvents are lower than unity, but are larger than unity for the other RTIL solvents as described in Chapter 4. On the other hand, the $\tau_R^{obs}/\tau_R^{slip}$ values of TEMPO, CProxylH, and $CProxyl^-$ are larger than unity. Therefore, rotation diffusion of pseudo-sphere solutes being larger than PADS can be explained by hydrodynamic theory with slip boundary condition.

Figure 5.2 shows the $\tau_R^{obs}/\tau_R^{slip}$ values for three RTILs as a function of the V_p values increase. The $\tau_R^{obs}/\tau_R^{slip}$ value seems to increase as V_p value decreases. The hydrodynamic theory with stick boundary condition holds for larger-sized solute/ smaller-sized solvent systems. The system in which V_p is large is close to the condition that hydrodynamic theory with stick boundary condition holds, and τ_R^{obs} values are close to τ_R^{stick} values.

(5.3.4) Volume and shape dependence of solute rotational correlation time in RTILs

The solute volume dependence was examined for rotational diffusion of pseudo-sphere solutes in RTILs in the above section. Here, solute shape dependence of $\tau_R^{obs}/\tau_R^{slip}$ values in RTILs is examined by using two prolate top solutes, PADS and DOXYL whose *f* values are different. Figure 5.3 (a) shows plots of $\tau_R^{obs}/\tau_R^{slip}$ values against *f* values for PADS samples and DOXYL in $BmimPF_6$. It is noteworthy that the $\tau_R^{obs}/\tau_R^{slip}$ value for DOXYL is lower than unity as well as PADS in $BmimPF_6$, which means neither PADS nor DOXYL in $BmimPF_6$ follow the present hydrodynamic theory

for rotational diffusion. This might suggest solvent shape as represented by *f* value is not important measure for understanding of the mechanism for rotational diffusion.

To evaluate rotation diffusion for DOXYL, Gierer and Wirtz (GW) theory[5] known as one of modified hydrodynamic theory for rotational diffusion is introduced. GW theory takes account of the discontinuous nature of the surrounding fluid for a dilute solution of spherical probe molecules in spherical solvent molecules and takes into consideration the relative sizes of the solute and solvent. Hence, rotational diffusion of solutes in RTILs are discussed on the basis of GW theory below.

According to GW theory, rotational correlation time is calculated by the following equation,

$$\tau_R^{GW} = \frac{V_p \eta}{k_B T} f C_{GW} \qquad (5.1)$$

where a coefficient C_{GW} for correction of viscosity around solute is given by

$$C_{GW} = \sigma_{GW}\left[6\sum_{m=1}^{\infty} \frac{\left(V_s / V_p\right)^{1/3}}{\left\{1 + 2m\left(V_s / V_p\right)^{1/3}\right\}^4} \right]^{-1} \qquad (5.2)$$

with σ_{GW} calculated the following equation.

$$\sigma_{GW} = \frac{\sum_{m=1}^{\infty} \left\{1 + 2m\left(V_s / V_p\right)^{1/3}\right\}^{-4}}{\sum_{m=0}^{\infty} \left\{1 + 2m\left(V_s / V_p\right)^{1/3}\right\}^{-4}} \qquad (5.3)$$

V_s is the volume of solvent. The V_s values of $BmimBF_4$, $BmimPF_6$ and $BmimTf_2N$ are 213.2, 247.5 and 326.5 $Å^3$ which are quoted from ref 6, 7. According to eqs (5.1) -

(5.3), the τ_R^{GW} values were calculated for PADS and DOXYL in $BmimPF_6$. The τ_R^{obs}/τ_R^{GW} values were calculated to compare the τ_R^{obs} and τ_R^{GW} values. Figure 5.3 (b) shows the τ_R^{obs}/τ_R^{GW} values plotted against V_{solute} values for PADS and DOXYL samples. The τ_R^{obs}/τ_R^{GW} value for DOXYL in $BmimPF_6$ is calculated to be 0.94, and the τ_R^{obs} value is almost the same as the τ_R^{GW} value. This means rotational diffusion for DOXYL in $BmimPF_6$ would be explained by GW hydrodynamic theory. Conclusively, the GW hydrodynamic theory may be adapted to evaluate the rotation motion of solutes with larger *f* values.

For PADS in $BmimTf_2N$, the τ_R^{obs}/τ_R^{GW} is 1.2 and the τ_R^{obs} value is longer than the τ_R^{GW} value. Therefore, the rotation motion for PADS in $BmimTf_2N$ can be also explained by GW theory. On the other hand, for PADS in $BmimBF_4$ and $BmimPF_6$, the τ_R^{obs}/τ_R^{GW} values are 0.25 and 0.34, respectively, and these are lower than unity. For PADS in $BmimBF_4$ and $BmimPF_6$, the τ_R^{obs} values are shorter than both τ_R^{slip} and τ_R^{GW} values. This may be caused by lowering of shear viscosity for the PADS rotational diffusion at high frequency as described in Chapter4, and because the other solutes are large and rotation diffusion is at low frequency, it may be not caused.

5.4 Conclusion

This chapter focuses on the effect of solute size and shape on rotational diffusion in RTILs. The solute size is represented by solute volume, V_p, and the solute shape is represented by *f* value which reflects the difference between hydrodynamic radii, $r_{//}$ and

$r_{\perp}$ for prolate top shape molecule as defined in Chapter 4. First, to discuss solute size dependence of rotational diffusion, the ratio of rotational correlation times determined experimentally (τ_R^{obs}) to those calculated by hydrodynamic theory with slip boundary conditions (τ_R^{slip}) were evaluated for solutes which indicate different V_p values and pseudo-sphere shape because f values is near unity. The $\tau_R^{obs}/\tau_R^{slip}$ values are found to be larger than unity for the solutes whose V_p is larger than that of PADS in RTILs. Next, to discuss solute shape dependence of rotational diffusion, the $\tau_R^{obs}/\tau_R^{slip}$ values were examined for two prolate top solutes, PADS and DOXYL whose f values are remarkably different. Both PADS and DOXYL show $\tau_R^{obs}/\tau_R^{slip}$ values of being lower than unity. To evaluate τ_R^{obs} value of DOXYL in $BmimPF_6$, another hydrodynamic theory proposed by Gierer and Wirtz (GW) was introduced instead of the hydrodynamic theory with slip boundary condition. The ratio of τ_R^{obs} value to rotational correlation time calculated by GW theory (τ_R^{GW}) equals to unity for DOXYL. On the other hand, the τ_R^{obs}/τ_R^{GW} values for PADS in $BmimPF_6$ and $BmimBF_4$ are lower than unity. These results indicate there are clear solute size and shape dependence for rotational diffusion of solutes in RTILs, and suggest the hydrodynamic theory with slip boundary condition is adapted to evaluate τ_R values for solutes which have larger V_p and pseudo-sphere shape, and the GW hydrodynamic theory is applicable to evaluate τ_R values for solute which has larger f value.

(a)

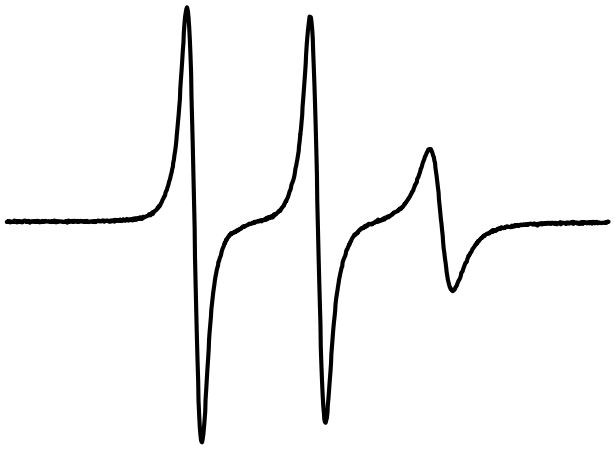

(b)

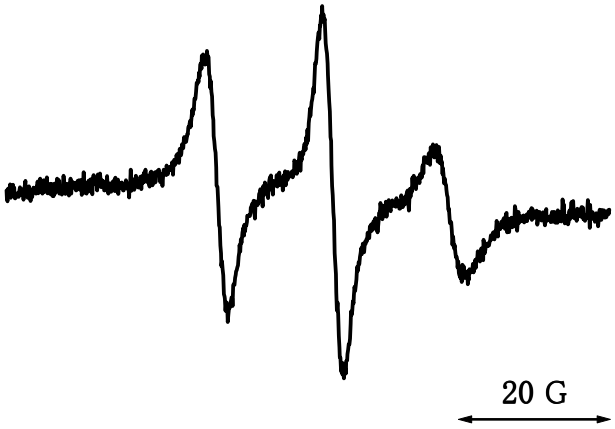

Figure 5.1: EPR spectra of nitroxide radicals in RTILs. (a) TEMPO in $BmimTf_2N$ at 270 K, (b) DOXYL in $BmimPF_6$ at 350 K

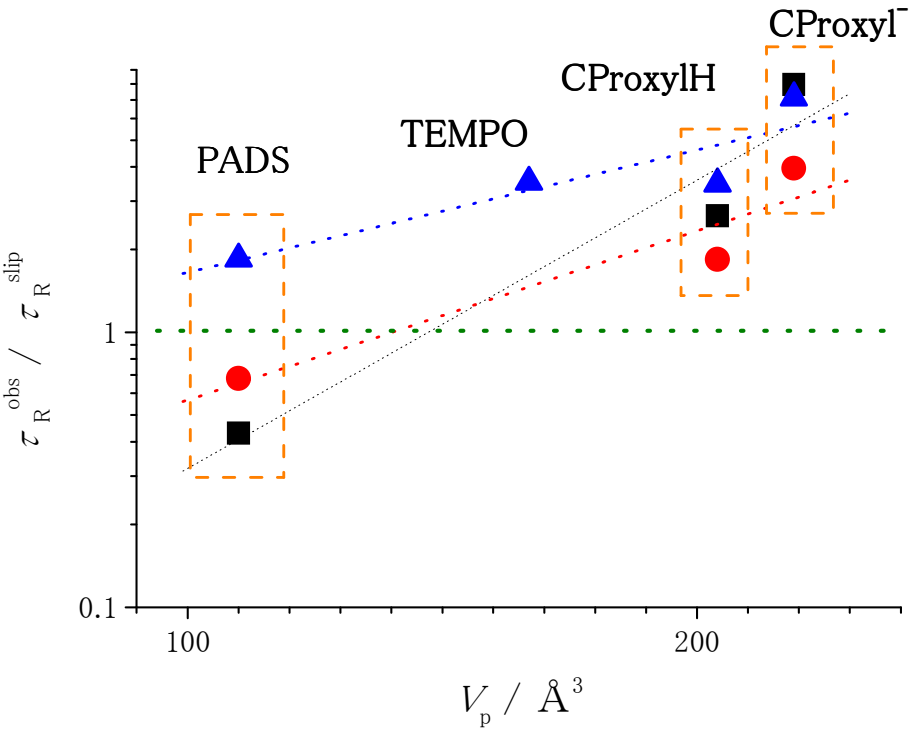

Figure 5.2: Plots of $\tau_R^{obs} / \tau_R^{slip}$ in log scale vs V_p. The solvents are $BmimBF_4$ (■), $BmimPF_6$ (●) and $BmimTf_2N$ (▲).

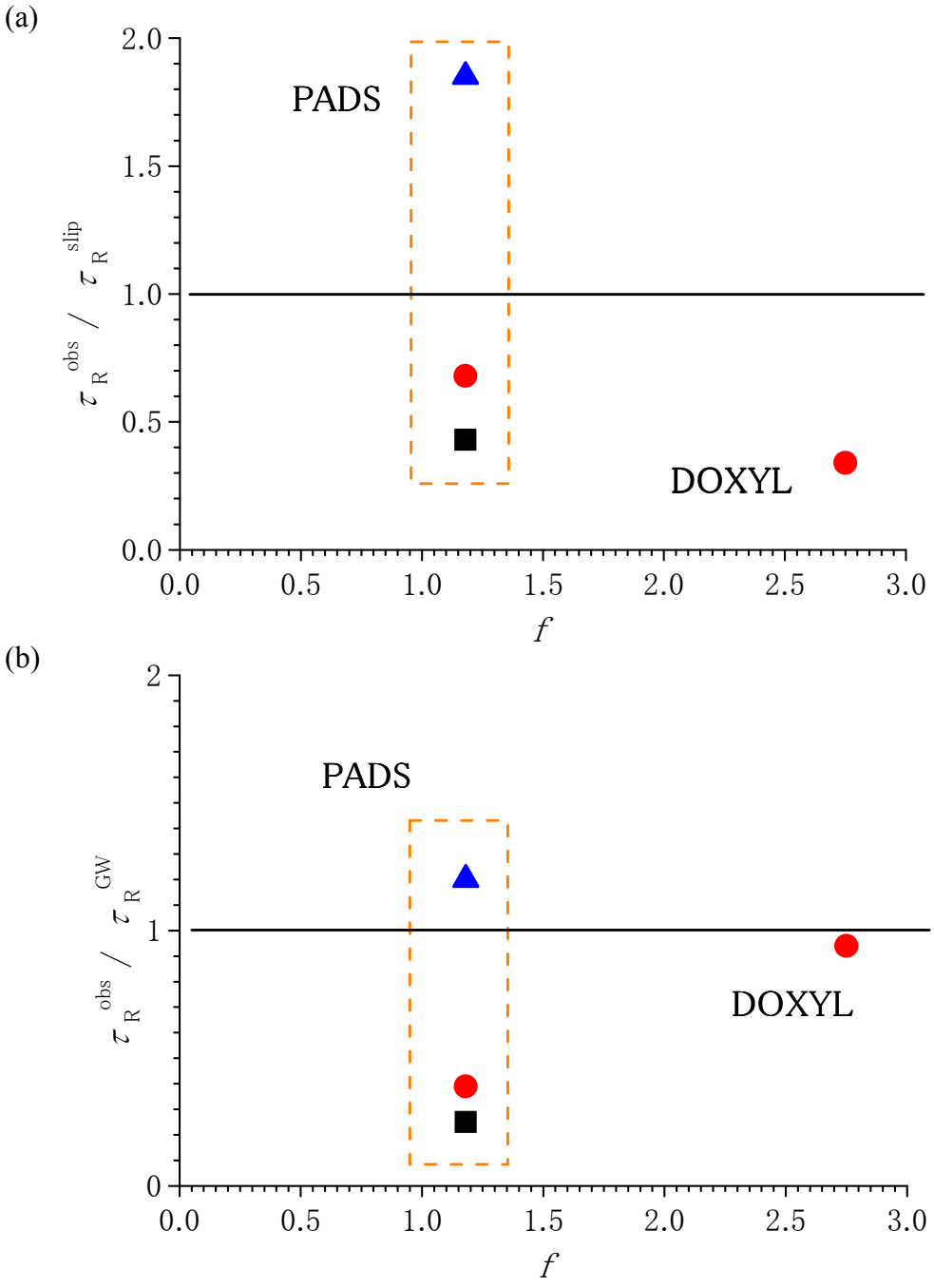

Figure 5.3: τ_R^{obs} / τ_R^{calc} vs f plots. The τ_R^{calc} values were calculated by (a) hydrodynamic theory with slip boundary condition and (b) Gierer and Wirtz hydrodynamic theory. The solvents were $BmimBF_4$ (■), $BmimPF_6$ (●) and $BmimTf_2N$ (▲).

Table 5.1: Comparison of $\tau_R^{obs}/\tau_R^{slip}$ values for solutes with different size of volume in RTILs

solute	V_{solute}/ Å^3	f	Solvent	T / K	τ_R^{obs}/ns	τ_R^{stick}/ns	τ_R^{slip}/ns	$\tau_R^{obs}/\tau_R^{slip}$
PADS	110	1.18	$BmimBF_4$	298	0.089	2.74	0.21	0.43
			$BmimPF_6$	298	0.47	9.4	0.70	0.68
			$BmimTf_2N$	298	0.18	1.3	0.098	1.9
TEMPO	167	1.08	$BmimTf_2N$	270	0.66	6.1	0.19	3.5
CProxylH	204	1.11	$BmimBF_4$	299	0.64	4.8	0.24	2.7
			$BmimPF_6$	298	1.5	16.4	0.82	1.8
			$BmimTf_2N$	294	0.46	2.6	1.3	3.5
$CProxyl^-$	219	1.09	$BmimBF_4$	298	1.2	5.0	0.15	8.0
			$BmimPF_6$	298	2.1	17.1	0.53	4.0
			$BmimTf_2N$	294	0.62	2.8	0.087	7.1
Doxyl	349[a)]	2.75	$BmimPF_6$	350	1.2	6.9	3.5	0.34

a) Taken from ref 8.

(a)

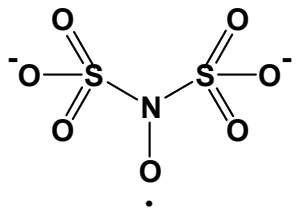

(b)

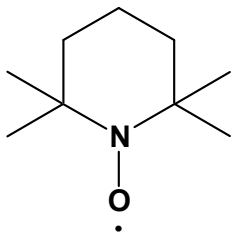

(c)

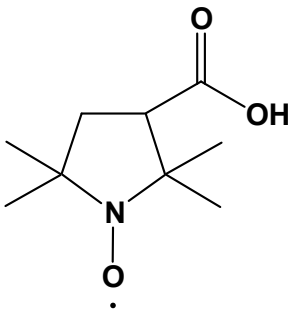

(d)

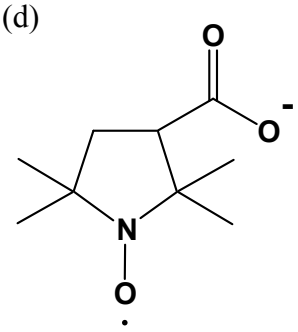

(e)

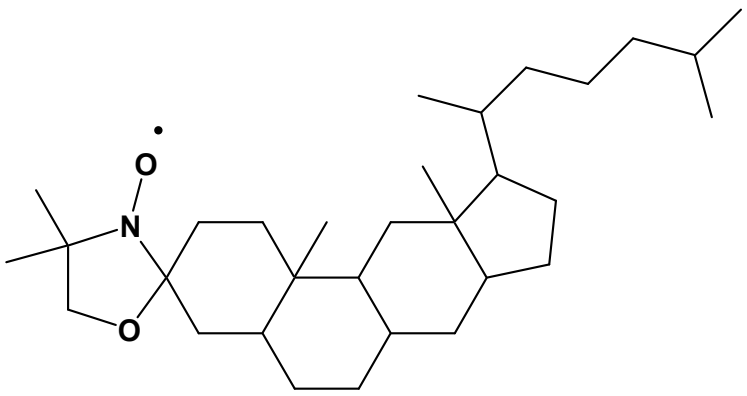

Chart 5.1: Structure of nitroxide radicals. (a) PADS, (b) TEMPO, (c) CProxylH, (d) CProxyl$^-$ and (e) DOXYL.

References of Chapter 5

(1) Ben-Amotz, D; Drake, J. M. *J. Chem. Phys*. **1988**, *89*, 1019.

(2) Roy, M.; Doraiswamy, S.; *J. Chem. Phys*. **1993**, *98*, 3213.

(3) Kowert, B. A.; Sobush, K. T.; Fuqua, C. F.; Mapes, C. L.; Jones, J. B.; Zahm, J. A. *J. Phys. Chem. A* **2003**, *107*, 4790.

(4) Poole, C. F. *J. Chromatogr. A* **2004**, *1037*, 49.

(5) Gierer, A.; Wirtz, K. *Z. Naturforsch. A* **1953**, *8*, 532.

(6) Jin, H.; Baker, G.; Arzhantsev, S.; Dong, J.; Maroncelli, M. *J. Phys. Chem. B* **2007**, *111*, 7291.

(7) Seki, S.; Kobayashi, T.; Kodayashi, Y.; Takei, K.; Miyashiro, H.; Hayamizu, K.; Tsuzuki, S.; Mitsugi, T.; Umebayashi, Y. *J. Mol. Liq.* **2010**, *152*, 9.

(8) Andreozzi, L.; Faetti, M.; Giordano, M. *J. Non-Crystalline Solids* **2006**, *352*, 3829.

Chapter 6. Summary and concluding remarks

Rotational diffusion of relatively larger-sized solutes dissolved in RTILs has been evaluated experimentally and can be understood in terms of hydrodynamic theory. The hydrodynamic theory is built under the conditions that the geometric size of solute is larger than that of solvent, and it is not obvious whether the rotational diffusion for smaller-sized solute obeys the hydrodynamic theory. In the present thesis the author focuses on the rotational diffusion of smaller-sized solute in RTILs. Rotational correlation times (τ_R^{obs}'s) of smaller-sized solutes dissolved in RTILs are derived by the aids of EPR spectroscopy and the resultant values are compared with those calculated by hydrodynamic theory (τ_R^{calc}'s).

In Chapter 3, the rotational dynamics of solutes in RTILs is examined by using proxyl radicals as an EPR spectroscopy probe. The τ_R^{obs} values of CProxylH in $BmimPF_6$ and $CProxyl^-$ in $BmimBF_4$ are successfully derived and compared with the τ_R^{calc} values calculated by a Stokes-Einstein-Debye (SED) hydrodynamic equation. Activation energies for τ_R^{obs} values are lower than those for the τ_R^{calc} values, which means that CProxylH in $BmimPF_6$ and $CProxyl^-$ in $BmimBF_4$ rotate more easily than the estimations by the SED equation. The dependence of τ_R^{obs} values on (η/T) is evaluated by a t–parameter defined as $\tau \propto (\eta/T)^t$. The t-values are found to be about 0.7 in RTILs, while they remain constant at unity in traditional organic solvents. This lower t value indicates that solutes rotate more easily than expected by the SED equation based on shear viscosity of solvent in $BmimPF_6$, and in $BmimBF_4$.

In Chapter 4, the rotation motion and solvation of PADS nitroxide radical dissolved in various RTILs are examined. The hyperfine coupling constant (A), the temperature-dependent anisotropic rotational correlation times ($\tau_{//}$ and $\tau_{\perp}$), and the rotational anisotropy (N) defined as $\tau_{\perp}/\tau_{//}$ are derived by analyzing the EPR spectra. The A values are constant for almost all RTILs, which indicates negligible interaction between the N-O group and the cation of RTILs. Next, the N values determined in RTILs and *N*-methylimidazole solvents are compared with the N value of 1.4 calculated by hydrodynamic theory. The N value of 2.4 for *N*-methylimidazole solvent is slightly larger than 1.4 but still close to the value calculated by hydrodynamic theory. On the other hand, the N values determined in RTIL solvents are 3 ~ 5 and apparently larger than 1.4. The interaction between the sulfonyl groups of PADS and the cation of RTILs seems to prolong the $\tau_{\perp}$ lifetimes in RTILs, which leads to larger N values in RTILs. Thirdly, experimental values of $\tau_{//}$ and $\tau_{\perp}$ are compared with those calculated by hydrodynamic theory. Almost all the experimental values are shorter than the calculated τ_R^{stick} values but longer than the calculate τ_R^{slip} values. The hydrodynamic theory with the slip boundary condition seems to give better agreement with the experimental τ_R^{obs} values. In some RTILs, experimental τ_R values are still shorter than the calculated τ_R^{slip} values. Finally, the t values are derived for all the samples. The t values are normally close to unity but the values below unity are derived from the experiments obtained in $BmimBF_4$, $BmimPF_6$ and $DemeBF_4$ solvents. On the basis of Debye relaxation of shear viscosity in $BmimPF_6$ reported recently, one plausible mechanism responsible for

the $t < 1$ relation observed in these RTILs is discussed.

In Chapter 5, the effect of solute size and shape on rotation diffusion in RTILs is examined. The solute size is represented by the volume ased on its geometric structure, V_p. The solute shape is represented by the anisotropic parameter (*f*-value), which reflects the difference between hydrodynamic radii, $r_{//}$ and $r_{\perp}$ for prolate top molecule. For the purpose to discuss solute size dependence of rotational diffusion, the ratios of τ_R^{obs} to τ_R^{slip} are evaluated for various solutes of different V_p values and pseudo-sphere shape ($f \sim 1$). It turns out that the $\tau_R^{obs}/\tau_R^{slip}$ values in RTILs are larger than unity for the solutes whose volumes are larger than that of PADS. In order to discuss solute shape dependence of rotational diffusion, the $\tau_R^{obs}/\tau_R^{slip}$ values are evaluated for two prolate top solutes, PADS and DOXYL whose *f* values are remarkably different. Both the $\tau_R^{obs}/\tau_R^{slip}$ values for PADS and DOXYL are found to be lower than unity. Gierer and Wirtz (GW) hydrodynamic theory is introduced instead of hydrodynamic theory with slip boundary condition. The ratios of the τ_R^{obs} value to rotational correlation time calculated by GW theory (τ_R^{GW}) are evaluated. The τ_R^{obs}/τ_R^{GW} ratios equal to be unity in the case of DOXYL, but the τ_R^{obs}/τ_R^{GW} values are lower than unity for PADS in $BmimPF_6$ and $BmimBF_4$. These results indicate solute size and shape dependence for the rotational diffusion in RTILs, and suggest the hydrodynamic theory with slip boundary condition is adapted to evaluate the τ_R values for the solutes of larger V_p and pseudo-sphere shape, while the GW hydrodynamic theory is adapted to evaluate the τ_R values for the solutes of larger *f* value.

In summary, it is concluded that rotational diffusion for smaller-sized solute in various RTILs can be understood by hydrodynamic theory with slip boundary condition in the same manner as the rotational dynamics for larger-sized solutes in traditional organic solvents. Nevertheless, the rotational diffusion for smaller solute in $BmimPF_6$ and $BmimBF_4$ and $DemeBF_4$ does not obey hydrodynamic theory. The author suggests that it can be explained by the relation between viscosity of the RTILs with small size anion such as PF_6 or BF_4 and the relatively fast rotational diffusion for proxyl radicals and PADS.

Appendix

τ_R^{obs} values of nitroxide radicals in RTILs

solute	solvent	T / K	τ_R^{obs} / ns
CProxyH	$BmimPF_6$	295	1.7
		298	1.5
		303	1.3
		307	1.0
		308	0.92
		312	0.82
		313	0.74
$CProxyl^-$	$BmimBF_4$	293	1.6
		294	1.5
		298	1.2
		303	1.0
		308	0.90
TEMPO	$BmimTf_2N$	270	0.66
DOXYL	$BmimPF_6$	350	1.2

$\tau_{\perp}^{obs}$,$\tau_{//}^{obs}$ and τ_R^{obs} values for PADS nitoxide radical in RTILs and a molecular solvent

solvent	T / K	$\tau_{\perp}^{obs}$ / ns	$\tau_{//}^{obs}$ / ns	τ_R^{obs} / ns
$BmimCH_3OSO_3$	298	1.3	0.27	0.58
	300	1.1	0.22	0.50
	305	0.82	0.17	0.37
	310	0.66	0.12	0.28
	315	0.49	0.099	0.22
	320	0.38	0.081	0.18
	325	0.31	0.061	0.14
	330	0.26	0.049	0.11
$BmimPF_6$	290	1.3	0.24	0.55
	295	1.0	0.22	0.47
	298	0.95	0.24	0.47
	300	0.71	0.15	0.33
	305	0.47	0.11	0.23
	310	0.38	0.093	0.19
	315	0.30	0.065	0.14
	320	0.23	0.054	0.11
$DemeBF_4$	305	1.8	0.39	0.82
	310	1.3	0.29	0.61
	315	0.86	0.22	0.44

solvent	T / K	$\tau_{\perp}^{obs}$ / ns	$\tau_{//}^{obs}$ / ns	τ_{R}^{obs} / ns
$DemeBF_4$	320	0.67	0.17	0.34
	325	0.53	0.13	0.26
$EmimC_2H_5OSO_3$	290	0.54	0.14	0.27
	295	0.41	0.095	0.20
	298	0.38	0.094	0.19
	300	0.31	0.075	0.15
	305	0.26	0.060	0.12
	310	0.20	0.043	0.092
	315	0.18	0.035	0.079
	320	0.14	0.029	0.064
$PP_{13}Tf_2N$	290	1.1	0.23	0.51
	295	0.77	0.19	0.39
	298	0.67	0.16	0.33
	300	0.60	0.17	0.32
	305	0.46	0.14	0.25
	310	0.34	0.10	0.18
	315	0.26	0.078	0.14
$BmimTf_2N$	290	0.38	0.10	0.19
	295	0.35	0.079	0.17

solvent	T / K	$\tau_{\perp}^{obs}$ / ns	$\tau_{//}^{obs}$ / ns	τ_{R}^{obs} / ns
$BmimTf_2N$	298	0.28	0.069	0.14
	300	0.26	0.062	0.13
	305	0.22	0.056	0.11
	310	0.17	0.050	0.092
	315	0.16	0.033	0.072
$EmimBF_4$	290	0.21	0.056	0.11
	295	0.17	0.043	0.084
	298	0.18	0.045	0.089
	300	0.15	0.038	0.075
	305	0.14	0.035	0.069
	310	0.12	0.025	0.054
	315	0.094	0.023	0.047
	320	0.081	0.015	0.035
$BmimBF_4$	280	0.36	0.11	0.20
	285	0.29	0.075	0.15
	290	0.24	0.056	0.12
	295	0.19	0.052	0.099
	298	0.17	0.048	0.089
	300	0.15	0.047	0.084

solvent	T / K	$\tau_{\perp}^{obs}$ / ns	$\tau_{//}^{obs}$ / ns	τ_{R}^{obs} / ns
$BmimBF_4$	305	0.14	0.029	0.064
	310	0.11	0.028	0.055
	315	0.11	0.024	0.051
	320	0.098	0.019	0.043
$Py_{14}Tf_2N$	285	1.2	0.34	0.65
	290	0.89	0.27	0.49
	295	0.47	0.18	0.29
	298	0.62	0.15	0.31
	300	0.61	0.14	0.29
	305	0.38	0.11	0.21
	310	0.28	0.076	0.15
	315	0.30	0.075	0.15
	320	0.19	0.065	0.11
$N_{3111}Tf_2N$	295	0.58	0.15	0.30
	298	0.42	0.15	0.26
	300	0.42	0.14	0.24
	305	0.34	0.10	0.19
	310	0.30	0.088	0.16
	315	0.22	0.069	0.12

solvent	T / K	$\tau_{\perp}^{obs}$ / ns	$\tau_{//}^{obs}$ / ns	τ_{R}^{obs} / ns
$N_{3111}Tf_2N$	320	0.19	0.055	0.10
	325	0.13	0.049	0.081
$Py_{13}Tf_2N$	290	0.44	0.14	0.25
	295	0.32	0.097	0.18
	298	0.28	0.082	0.15
	300	0.25	0.083	0.14
	305	0.21	0.068	0.12
	310	0.19	0.052	0.10
	315	0.14	0.048	0082
	320	0.12	0.035	0.065
$DemeTf_2N$	290	0.79	0.27	0.46
	295	0.61	0.22	0.37
	298	0.62	0.21	0.36
	300	0.50	0.16	0.28
	305	0.36	0.13	0.21
	310	0.29	0.10	0.17
	315	0.22	0.093	0.14
	320	0.21	0.068	0.12
N-methylimidazole	240	0.064	0.027	0.042

solvent	T / K	$\tau_{\perp}^{obs}$ / ns	$\tau_{//}^{obs}$ / ns	τ_{R}^{obs} / ns
N-methylimidazole	245	0.052	0.021	0.033
	250	0.045	0.018	0.029
	255	0.039	0.017	0.026
	260	0.038	0.015	0.024
	265	0.035	0.013	0.022

Acknowledgements

I wish to express my gratitude to Professor Kazuhiko Shibuya for his valuable advice and support. I am most grateful to Professor Akio Kawai for his helpful suggestion, valuable advice and encouragement. I am also obliged to Dr. Nobuyuki Akai for his helpful advice and encouragement. I also thank to Professor Tomoya Kitazume (Tokyo Institute of Technology), Dr. Shinichi Koguchi (Tokai University), Professor Yoshifumi Kimura (Kyoto University) and Professor Anunay Samanta (University of Hyderabad) for their unfailing advices.

I thank Mr. Tooru Asaka to measure NMR spectrum. I also thank Dr. Hajime Terazono, Dr. Masashi Tsuge, Mr. Takehiro Hidemori, Mr. Yutaka Marushima, Dr. Akira Ida, Mr. Yasuhiro Kawatani, Mr. Satoru Ohhisa, Mr. Takehiro Shiozaki, Mr. Takahiro Ogura, Mr. Masaki Iwama, Mr. Ryuta Aramaki and Mr. Atsushi Sugiyama for their helpful support and suggestion. Thanks are given to all the laboratory members for their various help.

Finally, I thank my father and mother for their kind supports and help.